



University of Kerbala
College of Science
Department of Chemistry

Electrodeposition of Ag, Sn and Mn from ionic liquids

A Thesis

Submitted to the Council of the College of Science/ University of Kerbala
In Partial Fulfillment of the Requirements for the Master Degree in Chemistry

Written by:

Duha Yahia Noori

B.Sc. Chemistry (2019) /University of Kerbala

Supervised by:

Asst. Prof. Dr. Hasan Fisal Alesary

Asst. Prof. Dr. Ahmed Hadi Al-Yasari

بِسْمِ اللَّهِ الرَّحْمَنِ الرَّحِيمِ

﴿ عَلَّمَ الْإِنْسَانَ مَا لَمْ يَعْلَمْ ﴾

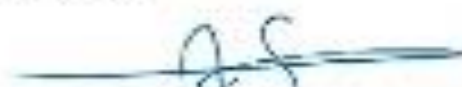
صدق الله العلي العظيم.

سورة العلق، آية: ٥

Supervisor Certification

We certify that this thesis " **Electrodeposition of Ag, Sn and Mn from ionic liquids**" was conducted under my supervision at the department of chemistry, College of science, University of Kerbala, as partial fulfillment of the requirements for the degree of Master of Science in Chemistry.

Signature:



Name: **Dr. Hasan-Fisal Alesary**

Title: Assistant Professor

Address: University of Kerbala,

College of Science,

Department of Chemistry.

Date: / / 2023

Signature:



Name: **Dr. Ahmed Hadi Al-**

Yasari

Title: Assistant Professor

Address: University of Kerbala,

College of Science,

Department of Chemistry.

Date: / / 2023

In view of the available recommendations by the supervisor, I forward this thesis for debate by the examining committee.

Signature:



Name: **Dr. Luma Majeed Ahmed**

Title: professor

Head of Chemistry Department, College of Science

Date: / / 2023

Examination Committee Certification

We certify that we have read this thesis entitled "Electrodeposition of Ag, Sn and Mn from ionic liquids" as the examining committee, examined the student "Duha Yahia Noori" on its contents, and that in our opinion, its adequate for the partial fulfillment of the requirements for the Degree of Master in science of chemistry

Signature:

Name: **Dr. Luma Majeed Ahmed**

Title: profesor

Address: University of Kerbala, College of Science,
Department of Chemistry.

Date: / / 2023

(Chairman)

Signature:

Name: **Dr. Sajid Hassan Guzar**

Title: professor

Address:

Date: / / 2023

(Member)

Signature:

Name: **Dr. Ahmeed Sadoon Abass**

Title: Assistant professor

Address:

Date: / / 2023

(Member)

Signature:

Name: **Dr. Hasan Fisal Alcsary**

Title: Assistant Prof

Address: University of Kerbala, College of
Science, Department of Chemistry.

Date: / / 2023

(Member & Supervisor)

Signature:

Name: **Dr. Ahmed Hadi Al-Yasari**

Title: Assistant Professor

Address: University of Kerbala, College of
Science, Department of Chemistry.

Date: / / 2023

(Member & Supervisor)

Approved by the council of the College of Science

Signature:

Name: **Dr. Jasem Hanoon Hashim Al-Awadi**

Title: Professor

Address: **Dean of College of Science, University of Kerbala.**

Date: 19 / 9 / 2023

Dedication

To my parents, for their love, support and prayers. To my brothers, Mustafa and Ali, and my sister, Tuka, who have been a source of encouragement to me. I dedicate this work.

Duha yahia Noori

Acknowledgments

Initially, I would like to thank Allah, for letting me through all the difficulties.

I would like to thank the following people, without whom I would not have been able to complete this research. I would like to express my deepest appreciation to my supervisors **Dr. Hasan Fisal Alesary** and **Dr. Ahmed Hadi** for their suggestion the idea of this project topic, insightful comments, support, and guidance. I am also thankful to **Dr. Azhar Al-Murshedi** for helping me to use the potentiostatic device to measuring the cyclic voltammetry (C.V). Also, I thank all faculty members of the Department of Chemistry in the College of Science at the University of Kerbala.

lastly, I would be remiss in not mentioning my family, especially my father and mother. Their belief in me has kept my motivation high during these years.

Abstract

Electrodeposition of metals has been used in the automotive and aerospace industries. Physical and mechanical properties of metal tools can be improved by depositing with metals have high resistance to corrosion. Sn, Ag and Mn are generally used for corrosion protective of steel plates or other metal pieces. Electrodeposition of metals was previously achieved in aqueous solution. However, the disadvantages of aqueous solutions limited the deposition of metals. The main objective of this study was to use of the green solvent (Ethaline200) during electrodeposition of Sn, Ag, and Mn with enhancement the quality of coating by using additives. In this work the effects of temperature and additives on the electrodeposition of Sn, Ag and, Mn from Ethaline 200 have been investigated. It was found that high temperature significantly effected on the morphology of Sn deposit, where produced homogenous film. Boric acid (BA) has improved the morphology of Sn. Moreover, the electrodeposition of Sn on different metallic substrate (copper, mild steel, and brass) has been achieved. Ag electrodeposition from Ethaline 200 (1ChCl:2EG) has been studied on different metallic substrate (copper, brass, and mild steel). it was found that type of substrate significantly affected the Ag deposits. electrodeposition of Ag more preferable on copper and copper alloy substrate than mild steel was observed.

The effects of potassium bromide (KBr) as inorganic additive on the electrodeposition of Mn from Ethaline 200 has been examined, and enhancement in the Mn deposition can be shown. Electrochemical properties of the plating liquid have been studied using cyclic voltammetry and the resultant surface characteristics such as morphology, composition and thickness were revealed by SEM/EDXS and AFM. XRD was used to examine the crystal structure of the Sn, Ag and Mn.

Subject		Page
Abstract		I
List of Tables		V
List of Figures		VI
List of Abbreviations		VIII
Chapter one introduction		
No.	Subject	Page
1.1	Electrodeposition	2
1.2	Ionic liquid	3
1.3	Deep Eutectic solvents (DESS)	4
1.4	Properties of Deep Eutectic Solvents (DESS)	8
1.5	Ethaline-based deep eutectic solvent	9
1.6	Metal electrodeposition from deep eutectic solvents	10
1.6.1	Sn electrodeposition	11
1.6.2	Ag electrodeposition	13
1.6.3	Mn electrodeposition	14
1.7	Electrocrystallization	15
1.8	Parameters' effects on the electrodeposition process	16
1.8.1	Role of Additives on Electrodeposition of Metals	17
1.8.1.1	Effects of Additives on Grain size of Deposit	18
1.8.1.2	Mechanisms of additives	18
1.9	Aims of this project	20
Chapter two Experimental part		
2.1	Materials and Chemicals	22
2.1.1	instruments	23
2.2	Preparation of Ethaline 200	23
2.3	Preparation of plating solutions	23

2.3.1	Preparation of Sn electrodeposition solution	23
2.3.2	Preparation of silver electrodeposition solution	24
2.3.2	Preparation of Mn electrodeposition solution	24
2.4	Electrodeposition processes	24
2.4.1	Electrodeposition of Sn	24
2.4.2	Electrodeposition of Ag	24
2.4.3	Electrodeposition of Mn	25
2.5	Measurement of physical properties	26
2.5.1	Measurement of conductivity	26
2.6	UV-Visible spectroscopy measurements	26
2.7	Electrochemical measurements	27
2.7.1	Cyclic voltammetry	27
2.8	Surface analysis	28
2.8.1	Scanning electron microscopy and energy dispersive X-ray analysis (SEM/EDX)	28
2.8.2	Atomic force microscopy	29
2.8.3	X-ray diffraction	30
Chapter three		
Results and discussion		
3.1	Tin electrodeposition	33
3.1.1	Physical Properties	33
3.1.2	Cyclic voltammetry	34
3.1.3.	surface analysis	36
3.2	silver electrodeposition	42
3.2.1	Conductivity	42
3.2.2	Cyclic voltammetry	43
3.2.3	Surface analysis	44
3.3	Manganese electrodeposition	49
3.3.1	Speciation	49
3.3.2	Conductivity	50

3.3.3	Cyclic voltammetry	51
3.3.4	Surface analysis	52
3.4	Conclusions	56
3.5	Future work	57
	References	58

List of Tables		
No.	Subject	Page
1. 1	types of DESs [20]	7
2. 1	chemicals and materials	22
2. 2	instruments and its model	23
3. 1	Average surface roughnesses of Sn films	39
3. 2	Average surface roughness of various Ag films	46
3. 3	Average roughness of the Mn deposits performed from Ethaline 200 containing of different amounts of KBr	54

List of Figures		
No.	Subject	Page
1. 1	classification of ionic liquids [8]	3
1. 2	A binary phase diagram for eutectic mixture [16]	5
1. 3	Comparison between DESs and ILs [17]	5
1. 4	Applications of DESs	6
1. 5	Molecular illustration of the arrangement of EG, [Ch] ⁺ , [Cl] ⁻ in bulk Ethaline. White, Blue, red, and cyan spheres represented hydrogen, nitrogen, oxygen, and carbon atoms, respectively. [27]	10
1. 6	schematic diagram of metal electrocrystallization [68]	16
1. 7	Shows adsorption of additives on active sites of surface of electrode [71]	19
2. 1	(a) the schematic diagram of Electrodeposition steps of (Ag/Sn/Mn)	25
2. 2	Conductivity meter device	26
2. 3	Schematic diagram showing cyclic voltammetry system [21]	28
2. 4	a) Schematic diagram of the scanning electron microscopy (SEM) principle, b) Energy dispersive X-ray spectroscopy principle [76]	29
2. 5	An illustration of the AFM instrument and a schematic diagram illustrating the principle of atomic force microscopy	30
2. 6	a) Schematic diagram of X-ray diffraction, b) schematic diagram of a diffractometer.	31
3. 1	(a) The viscosity (b) The conductivity of 0.1 mol L ⁻¹ SnCl ₂ ·2H ₂ O in Ethaline 200, at a range of temperature (25-90 °C) and various amounts of BA	34
3. 2	Cyclic voltammograms of 0.1 M SnCl ₂ ·2H ₂ O in Ethaline 200: a) different temperatures at a scan rate of 30 mV s ⁻¹ , b) different scan rates, and c) different concentrations of boric acid. All depositions were achieved using a Pt disc (working electrode), a Pt flag (counter-electrode), and Ag and Ag/AgCl (reference electrode).	35
3. 3	SEM images for Sn electrodeposited from 0.1 mol L ⁻¹ SnCl ₂ ·2H ₂ O in Ethaline 200. Both films were performed on a copper substrate and at a current density of 30 mA cm ⁻² , a) at room temperature, b) at 80°C.	37
3. 4	Visual photos, SEM morphologies, and AFM from left to right respectively of Sn films obtained from Ethaline 200 containing 0.1 mol L ⁻¹ SnCl ₂ ·2H ₂ O with and without various amounts of BA for 30 min. on a Cu substrate at 80 °C at 30 mA cm ⁻² current density. Image a) is for the Sn deposition without BA, with b) 0.01 M BA, c) 0.03 M BA, and d) 0.05 mol L ⁻¹ BA	38
3. 5	SEM images and EDX spectra for the electroplating of SnCl ₂ ·2H ₂ O (a) on a copper substrate, (b) on a brass substrate, and (c) on a mild steel substrate. All experiments were carried out at 80°C for 30 min.	40

3. 6	XRD patterns for Sn films from 0.1 M SnCl ₂ .2H ₂ O in Ethaline on mild steel, brass, and copper electrodes. All experiments were carried out for 30 min. at 80°C and at a current density 30 mA cm ⁻²	41
3. 7	Conductivity diagram of AgCl in Ethaline 200 different temperatures	42
3. 8	Cyclic voltammograms of 0.05 mol L ⁻¹ AgCl in Ethaline 200 on a Pt disc electrode (a) at different scan rates, (b) at different temperature	44
3. 9	Optical image (left), SEM images (middle), and EDX spectra (right) of Ag films obtained on (a) copper, (b)brass, and (c) mild steel substrates.	45
3. 10	AFM images of Ag films electrodeposited on different metallic substrates: (a) on copper, (b) on brass, and (c) on mild steel	47
3. 11	X-ray diffractograms of Ag films deposited from Ethaline 200 at 80 °C, 10 mA cm ⁻¹ current density, on different substrates copper, brass, and mild steel	48
3. 12	(a) optical image of 0.7 M MnCl ₂ .4H ₂ O in Ethaline 200 containing different concentrations of KBr, (b) UV-vis spectra for 0.7 mol L ⁻¹ MnCl ₂ .4H ₂ O in Ethaline 200 with different concentrations of KBr	49
3. 13	Conductivity of 0.7 mol L ⁻¹ MnCl ₂ .4H ₂ O in Ethaline 200 with different concentrations of KBr as a function of temperature	50
3. 14	Cyclic voltammograms of 0.7 mol L ⁻¹ MnCl ₂ .4H ₂ O in Ethaline 200 at 80°C using a Pt disc electrode, Pt flag electrode, and Ag electrode, (a) as function of scan rates, (b) with and without KBr at 5 mV scan rate	52
3. 15	SEM images and EDX spectra showing films electrodeposited from 0.7 mol L ⁻¹ MnCl ₂ .4H ₂ O in Ethaline 200 systems in the absence and presence of different concentrations of KBr (a) without, (b) with 0.05 mol L ⁻¹ KBr, and (c) with 0.1 mol L ⁻¹ KBr	53
3. 16	AFM images for the Mn deposit formed from Ethaline 200 (a) without KBr, (b) with 0.05 M KBr, and (c) with 0.1 M KBr	54
3. 17	XRD patterns for Mn deposits produced from 0.7 mol L ⁻¹ MnCl ₂ .4H ₂ O in Ethaline 200 with 0.05 mol L ⁻¹ and 0.1 mol L ⁻¹ KBr. All deposits were performed for 6 h. at 90 °C and at a constant potential of -1.75 V.	55

List of Abbreviations

Abbreviations	The Meaning
AFM	Atomic force microscopy
BA	Boric acid
CE	Counter electrode
ChCl	Choline chloride
CV	Cyclic voltammetry
DES	Deep eutectic solvent
E	Potential / Voltage
EDXS	Energy-dispersive X-ray spectroscopy
EG	Ethylene glycol
HBD	Hydrogen bond donor
IL	Ionic liquid
JCPDS	Joint committee on powder diffraction standards
Ra	Roughness
RF	Reference electrode
SEM	Scanning electron microscopy
UV-Vis	Ultra violet-visible light spectrophotometry
WE	working electrode
XRD	X-ray diffraction
θ	Bragg angle
λ	Wavelength(nm)
<i>i</i>	Current (A)

Chapter One

Introduction

Chapter one: introduction**1.1 Electrodeposition**

Metallic coatings play an important role in many applications such as automotive, aerospace, jewelry, and machinery. There are a variety of deposition methods including, as examples, thermal spray, laser technology, physical vapor deposition, and electrochemical deposition. Among them, electrodeposition is one of the more preferred on the industrial scale because of it is characterized by the diffusion of ions, resulting in the production of well-defined, high-quality surfaces. Additionally, exact layer thickness control, composition, and uniformity is well controlled, has a low production cost, and the morphology of the products are of high quality; these are all factors that make electroplating technology vital. [1]

In general, the term ‘electroplating’ indicates a process in which metallic or semiconducting films are formed on conductive substrates starting from metal ion precursors in a electrolyte, and which occurs via a charge transfer process. [2]

Metal electrodeposition is usually performed from aqueous solutions because the handling and chemistry of such baths is well known; however, not all metal coatings processes are possible via aqueous mediums [3]. Moreover, electrodeposition of metals from aqueous solution has several disadvantages: current efficiency is low, evolution of hydrogen, the electroplating of some elements requires toxic reagents such as cyanide, has a narrow potential window, electrodeposition of water-sensitive elements such as W, Al, and Ti can be extremely difficult, and some metals are poorly electrodeposited from aqueous electrolytes (such as Zn and Cr) [4]. In contrast to aqueous electrolytes, deep eutectic solvents, as a subclass of ionic liquids, have many advantageous properties for use in electrodeposition. Due to their wide potential windows for electrodeposition, ionic liquids can deposit at highly negative redox potentials metals. [5]

1.2 Ionic liquid

The term 'ionic liquid' indicates liquids that are entirely constituted by ions and exhibit a melting point that is lower than 100°C. Ionic liquids consist of asymmetric organic cations, for instance, alkyl phosphonium, *N,N*-dialkyl imidazolium, and *N*-alkyl pyridinium, and an inorganic anion such as, $[\text{PF}_6]^-$ or Cl^- . [6]

ionic liquids were prepared for first time by Walden et al., where ethylamine nitrate $[\text{EtNH}_3]^+ [\text{NO}_3]^-$ was synthesized, then ILs were obtained from *N*-ethyl pyridine bromide and aluminum chloride, but this type of ILs (first generation) was very sensitive to air and water. The second generation of ILs was prepared by using starting materials such as BF_4 and PF_6 as anions, where these ILs are limited in use on the commercial scale due to their high cost. The third generation is more renewable and more stable. [7] **Fig. 1.1**, show classification of ionic liquids.

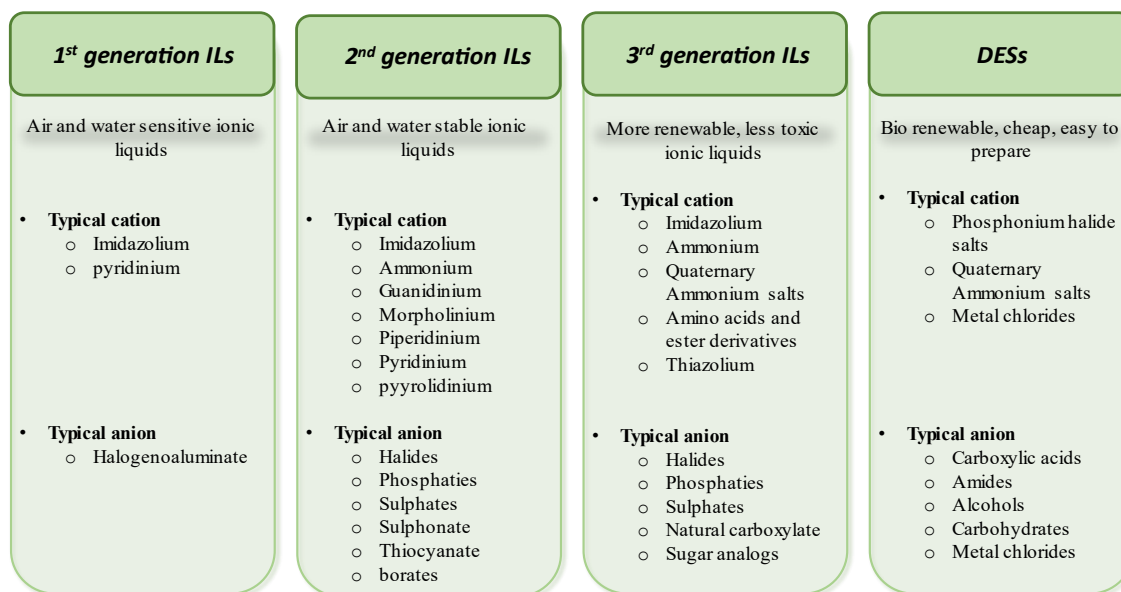


Figure 1. 1: classification of ionic liquids [8]

ILs are characterized by having very low vapor pressures, and as a result they are non-volatile; they are also highly polar and chemically inert. They are designer liquids and are reusable (can be separated by suitable procedures for example, can be removed under reduced pressure or extraction). ILs are applied in various fields, from catalysis and formation of metal nanostructures, to analytical and bioanalytical chemistry. [9]

Moreover, the main application of ILs is that of the electrodeposition of metals. The excellent solubility of metal salts, avoidance of metal/water chemistry, wide potential windows, and high conductivity in contrast to organic solvents are among the main strengths of the use of ILs in electrochemistry. [10]

1.3 Deep Eutectic solvents (DESSs)

“Deep eutectic solvents (DESSs) are binary mixtures of the definite composition of two components, one of which being ionic, that yield a liquid phase at ambient conditions, $\leq 25^{\circ}\text{C}$ ” [11]. This type of solvent was prepared for the first time about two decades ago by Abbott by mixing a 1 choline chloride:2 urea in molar ratio [12]. Later, researchers presented many new types of DESSs. In 2004, deep eutectic solvents were prepared using choline chloride with carboxylic acids. In 2007, metal salts were used instead of quaternary ammonium or phosphonium salts to prepare DESSs. These types of DESSs were formed between metal salts and simple alcohols or amides. Thereby, a new deep eutectic solvent system, which consisted of choline chloride with phenols at different molar ratios, was introduced [13].

All solid-liquid phases of mixtures are characterized by the presence of a eutectic point, while deep eutectic solvents are distinguished from other eutectic mixtures with the ‘deep’ title, which is due to their melting temperatures being assumed to be considerably lower than the ideal eutectic temperature, which is considered a key feature of these solvents [14, 15]. based on **Fig. 1.2**, at the eutectic point, the degree of freedom on the two components system is equal to zero, that demonstrated no change in chemical potential.

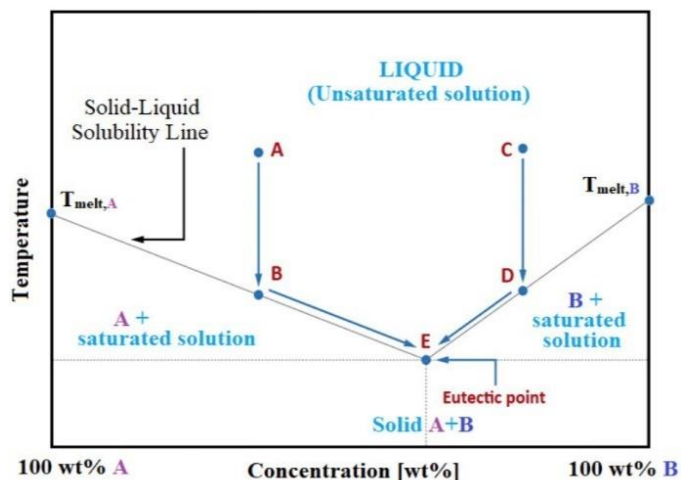


Figure 1. 2: A binary phase diagram for eutectic mixture [16]

DESs are a subclass of ILs because they are similar in physical properties but fundamentally different in chemical terms in two main ways: the nature of the raw materials, and the methods of their preparation. Figure 1.3 summarizes the most important similarities and differences between DESs and ILs [17].

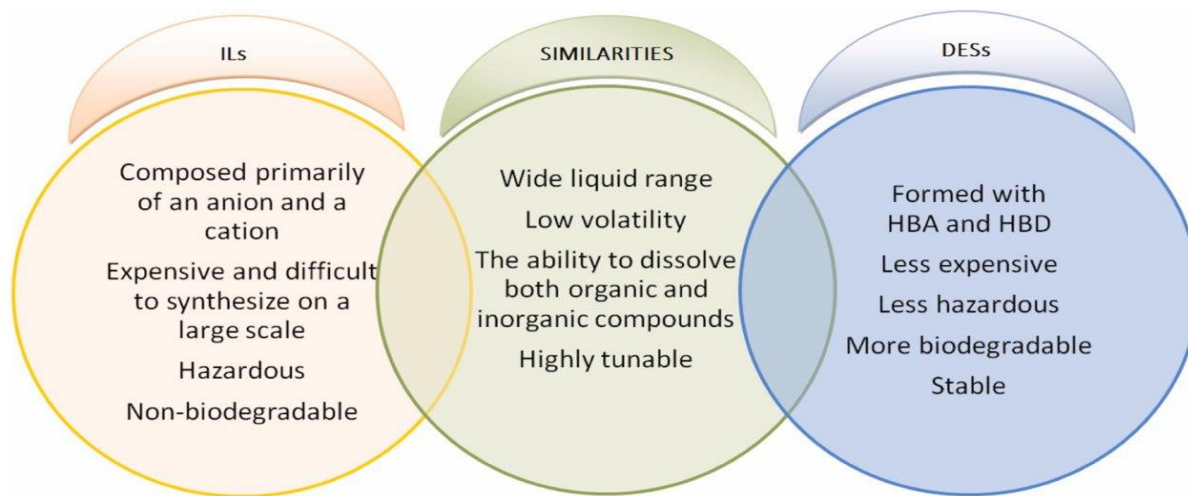


Figure 1. 3: Comparison between DESs and ILs [17]

In general, there are two easy approaches to preparing DESs. The first way involves melting the component that has the lower melting point and then adding the component with the higher. The second way, however, involves the mixing of the two components and then melting them together [13]. DESs have excellent physical properties such as ease of preparation, low toxicity, high biodegradability, and being inexpensive; furthermore, these solvents have significant designability (a broad range of anions, cations, HBD, and molar ratios of HBDs/salts), they have gained considerable attention in various industrial fields [18]. DESs have been used in a broad range of applications, such as the synthesis of metal nanoparticles and metal processing applications. Moreover, DESs have been used for the selective synthesis of organic compounds and also for electroplating processes [19]. **Fig 1.4** summarizes the major applications of DES.

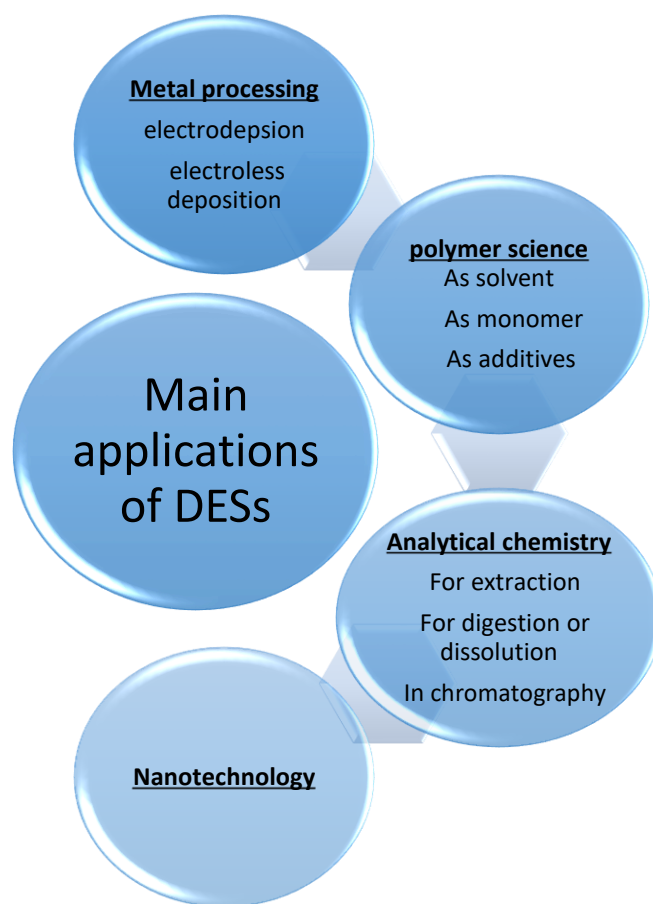


Figure 1. 4: Applications of DESs

Due to the variety of species that can be used to form DESs, they are classified into main four types, as shown in Table 1.1.

Table1. 1: types of DESs [20]

type	Formula
1	$\text{Cat}^+ \text{X}^- z\text{MCl}_x$
2	$\text{Cat}^+ \text{X}^- z\text{MCl}_x \cdot y\text{H}_2\text{O}$
3	$\text{Cat}^+ \text{X}^- z\text{RZ}$
4	$\text{MCl}_x + \text{RZ} = \text{MCl}_{x-1}^+ \cdot \text{RZ} + \text{MCl}_{x+1}^-$

Where: cat^+ indicates any ammonium, sulfonium, or phosphonium salt. X^- is generally a halide anion of a salt. M, metal. RZ, hydrogen bond donor. z, the number of molecules. [20]

Type 1 (quaternary salt and metal halide):- this type is formed from non-hydrate metal halides (such as: FeCl_2 , AgCl) and a quaternary ammonium salt. There are very few non-hydrated metal halides with suitably low melting points for this application. The only ones which form DESs with quaternary ammonium salts are FeCl_3 and ZnCl_2 . Some anhydrous metal salt-based DESs show low conductivities and high viscosities.

Type 2 (quaternary salt and hydrated metal halide):- in contrast to non-hydrated metal salts, hydrated salts are preferred in forming eutectic mixtures with quaternary ammonium salts, for instance, $\text{MgCl}_2 \cdot 6\text{H}_2\text{O}$, $\text{CrCl}_3 \cdot 6\text{H}_2\text{O}$, and $\text{CuCl}_2 \cdot 2\text{H}_2\text{O}$. Because the presence of water decreases the lattice energy, the melting point is decreased too. It is not possible to use these systems in the electroplating of low reduction potential metals like that Al because their limited potential window. [3]

Type 3 (quaternary salt with hydrogen bond donor):- this type of DESs are prepared by simply mixing a wide selection of hydrogen bond donors with quaternary ammonium salts. There are many advantages to these DESs: they can solvate a great many compounds of metal oxides and chlorides, the prepare process is easy, are low price, and high number of them are biodegradable.

Type 4 (metal halide and hydrogen bond donor):- similar to type 3, however, this group of DESs use a metal halide instead of quaternary ammonium salts with hydrogen bond donor such as urea or glycerol. These DESs are the most recently developed. [21]

1.4 Properties of Deep Eutectic Solvents (DESs)

1.4.1- Freezing point (T_f):- in general DESs are characterized by lower freezing points than those of their individual components. The depression of freezing point of DESs are affected by several factors, including the nature of the hydrogen bond donor (HBD). To prepare low freezing point DESs, the choice of the type of HBD is very important, for example, in the case of ChCl when urea is used as the HBD in the formation of a DES with a freezing point of 12 °C, but when thiourea is used as the HBD this gives the DES has higher freezing point (69 °C). The anion of choline-derived salts has an impact on the DES's freezing point, for example, when selecting urea as an HBD and a choline salt as HBA, the freezing point of the subsequent DESs decreases in the order $F^- > NO_3^- > Cl^- > BF_4^-$. On the other hand, no correlation was presented between the freezing point of a deep eutectic solvent and the melting points of its pure components.

1.4.2 Viscosity:- DESs have high viscosities compared to molecular solvents. Most of the DESs have a high viscosity at room temperature. which is due to the extensive network of hydrogen bond taking place between components of mixture. in fact, there are very broad range of DESs viscosities. For instance, deep eutectic solvents based on metal salts is known to have a very high viscosities (1 ChCl: 2ZnCl has a 85000 m pa. s). sugar- based deep eutectic solvents have a high viscosities (12730 m pa. s for 1:2 ChCl: sorbitol) while Ethaline200 has extremely low viscosity (37 m pa. s at 25 °C). Temperature has significant impact on viscosity, where viscosity is inversely proportional to temperature, which may be due to increasing temperature leading to a weaker bonding between the HBD and choline cation. The size of the ion also has an important effect on viscosity, thus to produce DESs with highest mobility the ions need to be relatively small. Moreover the nature of components, their molar ratio, and content of water can all influence the viscosity of DESs. The impurities can also affect the value of the viscosity. [22, 23]

1.4.3 Conductivity:- conductivity is related to viscosity. DESs with low viscosities have tens of mS/cm conductivity; however, for high viscosity DESs, a significant lowering in conductivity is observed. In general, conductivity increases with increasing quantity of salts, but there are

DESs that appear to deviate from this general trend: for instance, ChCl:EG has a maximum conductivity that decreases after a certain salt concentration is reached. A Walden plot can show the relationship between conductivity and viscosity, as plotted in the form of molar conductivity against fluidity, which is the inverse of viscosity. Walden rule $(\Lambda\eta = \text{constant})$, where η represent the viscosity and Λ indicates to molar conductivity [3]

1.5 Ethaline-based deep eutectic solvent

Ethaline, as a subclass of type 3 DESs, is a composite of choline chloride ((2-hydroxyethyl) trimethylammonium chloride) [melting point, $T_m = 302^\circ\text{C}$] with ethylene glycol [melting point, $T_m = -13^\circ\text{C}$], which serve as the HBD. This mixture is a liquid at room temperature. [24]. The choline cation, which is a component part of vitamin B, is manufactured in large amounts as a nutritional supplement for livestock. It is cheap, non-toxic, plentiful, and environmentally friendly, all of which make it a preferred HBA. [16]. Ethaline is characterized by having good solvation properties and a very low melting temperature. [25] Moreover, it has low viscosity and high conductivity, in contrast with other deep eutectic solvents such as reline and glyceline; it also has high biodegradability and low toxicity. [26]

Ethaline sees use in multiple fields, for instance, metal electroplating, metallic processing, electropolishing, improvement of drug solubility, and gel electrolytes. Due to the fact of its associated high current efficiency and low corrosion, Ethaline has been successfully used to achieve stainless steel electropolishing and obtain improved results for the electrodeposition of copper and tin. [27]

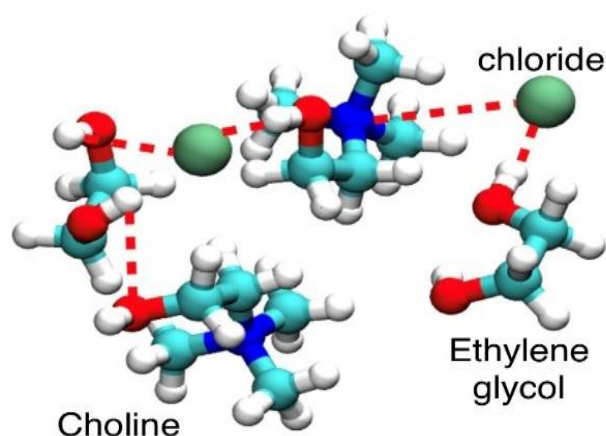


Figure 1. 5: Molecular illustration of the arrangement of EG, [Ch]⁺, [Cl]⁻ in bulk Ethaline. White, Blue, red, and cyan spheres represented hydrogen, nitrogen, oxygen, and carbon atoms, respectively. [27]

1.6 Metal electrodeposition from deep eutectic solvents

The electrodeposition technique is used to functionalize a surface in order to obtain required properties, for instance, hardness, wear and corrosion resistance, magnetism, brightness, and abrasion. Metal electrodeposition is usually performed from aqueous solutions because of their handling and bath chemistry is well known; however, not all metal coating processes are possible using aqueous baths. [3]. In contrast to aqueous electrolytes, deep eutectic solvents, as a subclass of ionic liquids, have many advantageous properties for use in an electrodeposition. Due to their wide potential windows, ionic liquids can deposit very negative redox potential metals. [5]

DESs have a high solubility for metal salts, including metal hydroxides and oxides, and can thus allow the production of thick coatings and help avoid passivation of substrates, electrodes, and deposits, unlike aqueous solutions in which the formation of non-soluble oxides and hydroxide layers on the electrode is commonplace and through which it is difficult to produce thick metal

films [22]. DESs' low vapor pressures and good thermal stabilities make them capable of deposition of materials that need a high-temperature bath. [28]

Although DESs have similar physicochemical properties to ILs, they have other excellent properties that make them preferable for the electrodeposition of metals on a large industrial scale:

(a) DESs are inexpensive and have a much-reduced environmental impact, whereas ILs are more expensive, are commonly toxic, and generally have poor biodegradability, biocompatibility, and sustainability.

(b) synthesis process is easy, simply mixing of constituents, no waste, with no purification steps required; however ILs, synthesis is more difficult and expensive. [20]

Since their inception, DESs have been utilized as electrolytes for deposition of metals (among a variety of their applications). Thin films, magnetic metal and alloy deposits, gallium and indium together as precursors for photovoltaic compounds, and composites (such as silica and alumina) have all been deposited from deep eutectic solvents. Many species of DESs have been used in electroplating process studies such as glyceline, ChCl/propylenegcol, ChCl/oxalic acid, ChCl/malonic acids and ChCl/CrCl₃.6H₂O; however, Reline (ChCl/urea) and ethaline (ChCl/EG) are more commercially available and have the widest range of possible applications. [29]

1.6.1 Sn electrodeposition

The electroplating technique is used to deposit many kinds of metals and alloys because it possesses various advantages, low processing temperatures, normal handling pressure, and the high purity of any resultant deposits [30]. Due to being nontoxic, ductile, and corrosion-resistant, tin and its alloy coatings are very important in various industrial fields [31].

Tin is used as an anode material in lithium ion rechargeable batteries, and as a coating to protect metals from corrosion. Tin is also used in foodstuff process [32]. Previously, the electrodeposition of tin was achieved from acidic solutions (such as methane sulfonic acid, fluoborite, and phenol sulfonic acid), or from alkaline solutions; however, the major drawback of alkaline solutions is that the deposition of tin must be carried out at elevated temperature.

The problem with acidic baths is the formation of a precipitate of tin oxide, SnO_2 [33, 34]. Moreover, the electrodeposition of metals from aqueous solutions have several disadvantages: current efficiency is low, hydrogen is evolved, the electroplating of some elements requires toxic reagents such as cyanide, a narrow potential window, difficult electrodeposition of water-sensitive elements such as W, Al, and Ti, and some metals are poorly electrodeposited from aqueous electrolytes (such as Zn and Cr). [4]

Various ILs have been utilized for electrodeposition of tin such as 1-n-methylpyrrolidinium bis(trifluoromethyl sulfonyl)imide (BMPTFSI) [35] and 1-ethyl-3-methylimidazolium dicyanamide (EMI-DCA)[36]; however, the major drawbacks of these liquids are their reactivity with water, their possible degradation in an oxygen environment [37], and the high cost of many ionic liquids.

Recently, DESs, which are a subclass of ILs, have been used in electrodeposition processes as an alternative solvent. DESs have some major advantages over conventional ionic liquids: they are easy to prepare, cheaper, biodegradable, and less toxic [38]. Among the various applications of DESs, they are widely used as electrolytes in electrodeposition processes [39-48]. Porous Sn film electrodeposition from Ethaline and its lithium storage performance were investigated by Gu et al. [49].

Sonia and coworkers studied the electrodeposition of tin from choline chloride with different HBD, showing that choline chloride-based solvents can be perfectly employed for the electrodeposition of tin [50].

SnCl_2 concentration can also have an effect on the formation of complexes in Ethaline, where Swatilekha et al. observed that there appears to be two stripping steps in polarization scans with increasing concentrations of tin salt ($\text{SnCl}_2 \cdot 2\text{H}_2\text{O}$) due to the formation of complexes such as SnCl_3 and Sn_2Cl_5 [51].

Cao et al. investigated the electrodeposition of tin from ChCl-urea-based DESs and studied the influence of temperature and concentration of SnCl_2 on their reduction behavior [52]. Tin alloys were also studied, where a tin-bismuth alloy was investigated by Vieira et al. [34].

1.6.2 Ag electrodeposition

Silver plating is of industrial importance as it is used in electrocatalysis, accumulators, the automotive and aerospace industries, jewelry, and for decorative purposes [52]. It has magnificent antibacterial and physicochemical features, excellent corrosion resistivity, and elevated bulk conductivity [33].

Silver can be deposited using various methods: electrodeposition, electroless plating, or vacuum techniques such as physical and chemical vapor deposition. However, physical and chemical vapor deposition methods suffer from multiple defects such as slow rate of deposition, the requirement for costly equipment, and challenges in controlling the quality of the product. Among all of these ways, electroplating is the best technique: it is the easiest and cheapest manner to yield good-looking, homogenous, and thin silver coatings [53].

Industrially electroplating of silver is performed in aqueous environments; however, these solvents are extremely toxic due to the large cyanide content used, where cyanide acts as a complexing agent to Ag^+ ions to prevent their spontaneous reduction [54].

Electrodeposition of metals from environmentally friendly liquids is a subject that has recently gained significant interest. Many ILs have been studied as alternative solvent to conventional toxic aqueous electroplating baths in Ag electroplating. Roberta et al. studied the electroplating of Ag from 1-butyl-3-methylimidazolium tetrafluoroborate ([BMIM][BF₄]). It was found that adherent, very thin, and pure Ag films could be obtained from such [53].

Pyrrolidinium-based ionic liquids such as *N*-butyl-*N*-methylpyrrolidinium bis(trifluoromethane sulfonyl)imide ([C₄mPyr][TFSI]) have been used in Ag electrodeposition; however, this process requires ambient conditions because [C₄mPyr][TFSI] is very sensitive to atmospheric water [54].

Silver deposits from the butylpyridinium dicyanide (pyriu-DCA) IL have also been reported by Sarra and co-workers [55].

1.6.3 Mn electrodeposition

Manganese alloys have been utilized as coatings in magnetic materials, corrosion-resistant materials, and semiconductors. Many implementations such as electrochemical glucose sensors, metal-air batteries, fuel cells, and supercapacitors use Mn-based materials [56] such as Al-Mn alloy coatings that can be used to enhance the corrosion resistance of NdFeB magnets [57]. Ni-Mn alloy coatings also appear to have more plasticity and mechanical strength compared to pure Ni deposits, where Mn increases the strength and temperature-resistance of Ni [58], as well as among Zn alloys where Zn-Mn alloy appears to have an extremely high corrosion resistance [59].

Mn electrodeposition from aqueous solution is challenging because of the high reduction potential of Mn ($\text{Mn}^{2+}/\text{Mn} = -1.18 \text{ V vs. SHE}$), which, alloyed to simultaneous hydrogen evolution, results in low current efficiency. In order to remove this drawback, sulfur or selenium species have been used as additives in the Mn electrodeposition bath, where selenium and sulfite (SO_3^{2-}) inhibit hydrogen evolution, increase the manganese current efficiency, and thus improve manganese film quality. However, Se compounds have a negative effect on the environment, worker health, and damage the workplace [60, 61].

N-butyl-*N*-methyl pyrrolidinium dicyanamide (BMP-DCD), butyl methyl pyrrolidinium bis((trifluoromethyl)sulfonyl) imide (BuMePy-TFSI), and butyl methyl pyrrolidinium bis(trifluoromethyl sulfonyl) imide (BMP-NTF₂) ILs have been used in the electrodeposition of pure Mn. The authors found that the electrodeposition temperature and potential can have an effect on Mn deposit and the amorphous nature of the Mn so obtained. [62-64]

As mentioned previously, due to the excellent properties of ChCl-based DESs, they show great potential for use in metal electrodeposition. Electrodeposition of Mn has been achieved in ChCl: urea-based DESs by Benedetto et al. [65].

Recently, Subrat et al. [66] used sodium alkyl sulfates (SDS, SLS, STS) as additives instead to selenium compounds in the electrodeposition of Mn from aqueous solution

William et al. examined the effects of glycine on the electroplating of Mn from ChCl:urea. They stated that glycine can inhibit the deposition of Mn. [67]

Thiourea (TU), as an organic additive, has also been used in the electrodeposition of Mn from ChCl:EG. It was found that TU induces the formation nanoflake architectures with a nanoporous configuration of Mn [56]

1.7 Electrocrystallization

Electrocrystallization term refers to metal deposition through electrochemical process. In general the steps of metal electrodeposition on substrate can be summarized as follows:

- Reactant transported to the interface region by convective diffusion. Electrocrystallization process is effect by changes in the interfacial layers, the interactions between these layers make the system environment is complex. The interface region is consist three zones: electrical double layer, concentration profile layer, and fluid velocity layer.
- Ion adsorption, electron transfer takes place on the active sites of substrate surface. Active sites represent the surface imperfections (involves stepped vicinal, high indexed surfaces, planes with a high density of kink sites) and oxidation / reduction of surface, adsorption/ desorption of solvent molecules or anions on the surface substrate, or surface reconstruction processes. After the ion deposition on any place of substrate as an adatom, it migrates to the growing site through surface diffusion.
- The spread of a nucleus by way of continued incorporation of monomer is called growth. The morphology and crystal structure of final deposit are depending on the direction of growth. The growth of thin film on a surface rely upon the energy of interaction between adatom-substrate and adatom-adatom [68]. **Fig. 1.6** shows the main steps of metal electrocrystallization.

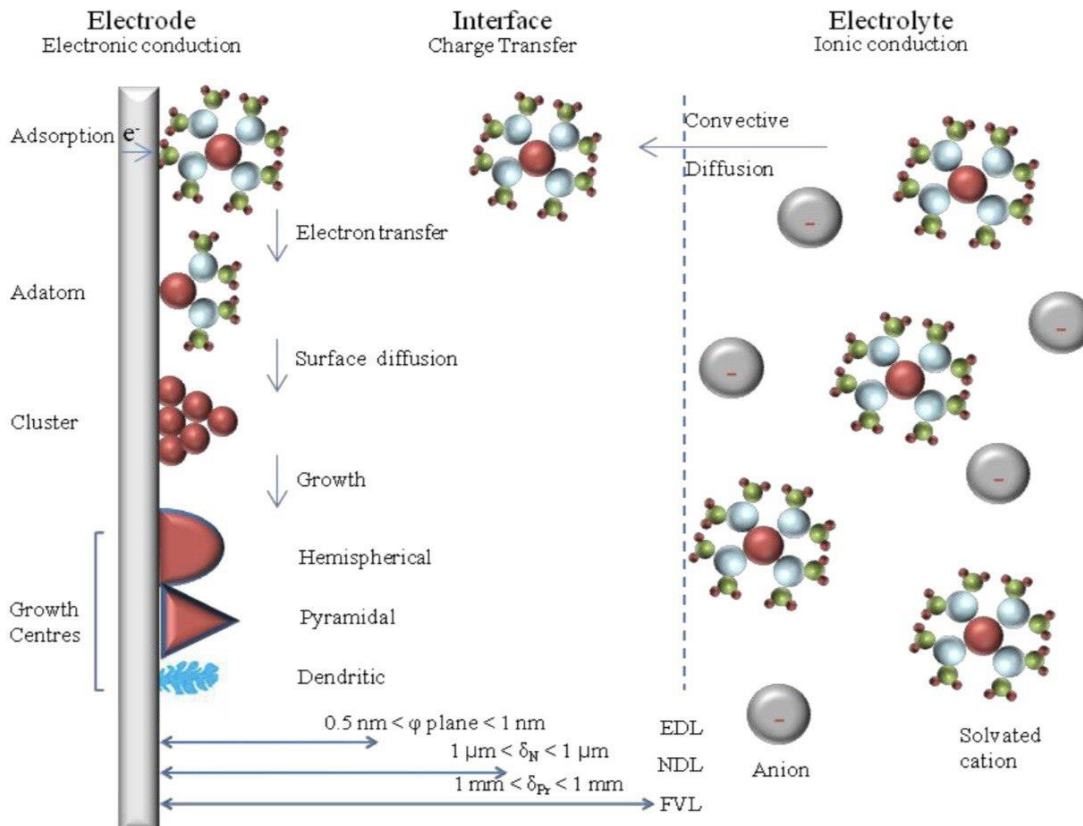


Figure 1. 6: schematic diagram of metal electrocrystallization [68]

1.8 Parameters' effects on the electrodeposition process

Electrode potential and current density, to temperature, pH, substrate, and concentration and type of metal salt are all parameters that can affect the electroplating process. Some of these factors can be summarized as per below:

Temperature has a considerable impact on the electrodeposition process. High temperature improves the conductivity of the solution and also increases the rate of electrochemical processes. In general, the upper limit of temperature which can be used in electrodeposition from DESs is 150-200°C. On the other hand, in aqueous baths, temperatures above 70°C may well accelerate the evaporation of the solvent and corrosion processes, limiting the practical temperatures achievable. Furthermore, an increase in temperature stifles additive

adsorption, decreasing their efficacy as a consequence, and deposits become more coarse-grained [69]. Many studies involving the effect of temperature on DES-based metal plating have been undertaken. For example, the influence of temperature on the morphology of indium depositions was studied by Ana et al., where it was observed that the particle size of the indium deposit decreased with increasing temperature. When electrodeposition was carried out at a temperature range of 25-65°C, the indium grains and rods obtained were in the micrometer regime. At 80°C, uniformly distributed nanorods of indium were obtained [70].

The substrate surface also affects the deposit structure, especially during the initial steps of electroplating process. This is due to the fact that the nucleation rate on the substrate differs from that on the freshly plated deposit [10, 69].

1.8.1 Role of Additives on Electrodeposition of Metals

Use of additives is one of the main factors that affects the electroplating process. In addition to effects on the grain size of the electrodeposition, which in turn significantly affects physical and mechanical properties such as wear-resistance, electrical resistivity, and hardness, additives can affect the polarization of the cathode, change of orientation of crystals, as well potentially incorporating metals in the deposit. The additives that have been used in metal electroplating are classified according to their effect on the deposit into two types: levelling agents, and brightening agents [71, 72]. Several researches have described the use of additives to enhance the electroplating of metals from the DES. For example, small molecule additives (nicotinic acid (NA), *p*-benzoquinone (BQ), boric acid (BA)) were used for zinc electroplating from ChCl:EG-based DES. It was found that a bright Zn deposit was obtained when nicotinic acid was used [40].

1.8.1.1 Effects of Additives on Grain size of Deposit

Crystal size plays a significant role in refinement of the deposit. It is found that levelling and brightening deposit depend on size of grain or crystal of metal. Brightening and levelling deposit can be obtained when the size of the metal crystal is smaller. The additives can refine the grain size where this can be occurred by blocking the cathode surface through adsorption of an additive agent. Thus, the additives impede grow big crystals this means that additives control in size of crystals

1.8.1.2 Mechanisms of additives

Smooth coating can be obtained by adding suitable agents to the plating bath. Some of studies have been made on the mechanisms of levelling of nickel and copper plating. Theory of levelling has been explained in papers by Kardos where the organic additive can be adsorbed on the electrode surface “blocking surface”. Thus, deposition of metal cannot take place on the sites occupied by the organic molecules. The levelling molecules will be adsorbed on the active sites or on the high points of electrode surface whereas at these high points thickness of diffusion layer less than in the recesses thus additive molecules will be transported faster. Consequently, adsorption of additive molecules in the recesses will be much less. Therefore, the metals tend to deposit in the recesses of electrode surface, and this is clear in **Fig. 1.7**.

Brightness is related to smooth surface which is able to reflect visible light whereas roughness of the surface should be less than 400 nm. Or brightening can be defined as the ability of solution to deposit crystals that have size smaller than the wavelength of visible light which are normally smaller than 400 nm. Small crystals are an essential for brightness but this cannot be a satisfactory condition. Some studies found that the brightness depend on the orientation of crystallites that are deposited on the surface in the same plane. Some organic compounds can be correlated with the metal forming complexes and this refines the metal crystals. These compounds usually have a sulphur atom bonded directly to carbon atom or consist of triple bond.[73]

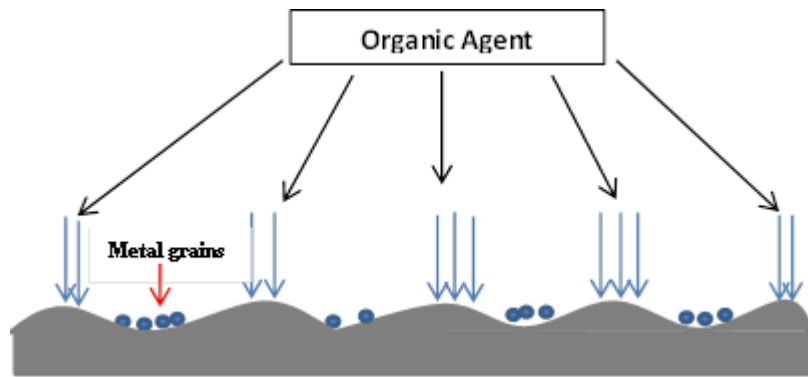


Figure 1. 7: adsorption of additives on active sites of surface of electrode [71]

1.9 Aims of this project

1. Studying effect of additives on the electrodeposition of Sn, Ag, and Mn in Ethaline 200 based deep eutectic solvent (DESs)
2. Studying speciation and the physical properties such as a conductivities for the plating liquids
3. Studying of electrochemical properties of Sn, Ag, and Mn species in Ethaline 200 using cyclic voltammetry method (CV)
4. Improvement physical properties of metals coatings such as brightness, thickness and roughness

Chapter Two

Experimental part

Chapter two: Experimental part**2.1 Materials and Chemicals**

All chemicals used in this work are listed in Table 2-1

Table 2. 1: chemicals and materials

No	Materials	Chemical Formula	Company supplied	Purity and percentage
1	Choline chloride	$\text{HOC}_2\text{H}_4\text{N}(\text{CH}_3)^+_3\text{Cl}^-$	Biochem Chemopharma	$\geq 98\%$
2	Ethylene glycol (EG)	$\text{C}_2\text{H}_4(\text{OH})_2$	Thomas baker	99%
3	Tin chloride dihydrate	$\text{SnCl}_2 \cdot 2\text{H}_2\text{O}$	SDFCL	97 %
4	Silver chloride	AgCl	Reagent world	99%
5	Hydrochloric acid	HCl	Fisher	$\geq 37.0\%$
6	Manganese chloride tetrahydrate	$\text{MnCl}_2 \cdot 4\text{H}_2\text{O}$	SDFCL	99%
7	Potassium bromide	KBr	NANIWA	99 %
8	Ammonium persulphate	$(\text{NH}_4)_2\text{S}_2\text{O}_8$	Sigma	$\geq 98\%$
9	Alumina	Al_2O_3	Fisher	$\geq 100\%$
10	Boric acid	H_3BO_3	NANIWA	99.8%

2.1.1 instruments

Instruments which were used in this study, are listed in table 2.2.

Table 2. 2: instruments and its model

No.	The instrument	Model	Work sites
1	Conductivity meter device	(DDS-22C)	Iraq- university of Kerbala
2	UV-Vis spectrophotometer	UV-1800	Iraq- university of Kerbala
3	Potentiostate	PGSTAT20	Iraq- University of Kufa- College of education for Girls
4	Scanning electron microscopy and energy dispersive X-ray analysis	TESCAN (MIRA 3)	Iran- University of Tehran
5	Atomic force microscopy	NTEGRA (NT-MDT)	Iran- University of Tehran
6	X-ray diffraction	Philips (PW1730)	Iran- University of Tehran

2.2 Preparation of Ethaline 200

Ethaline 200 as an electrolyte was prepared by mixing a 1:2 molar ratio of choline chloride (ChCl):Ethylene glycol (EG) at 70°C for about 30 minutes until a colorless, homogeneous solution was obtained.[71]

2.3 Preparation of plating solutions

2.3.1 Preparation of Sn electrodeposition solution

A) The tin electrodeposition solution without additives was prepared by mixing 80 ml Ethaline 200 with $\text{SnCl}_2 \cdot 2\text{H}_2\text{O}$ at a concentration of 0.1 mol L^{-1} and at 80°C with stirring continuously.

B) (0.01, 0.03, 0.05) mol L^{-1} of boric acid were individually added to the Sn electrodeposition bath

2.3.2 Preparation of silver electrodeposition solution

0.05 mol L⁻¹ of AgCl was prepared in 80 ml of (Ethaline 200) at 80°C to obtain a colorless and homogeneous solution.

2.3.2 Preparation of Mn electrodeposition solution

A) Mn electrodeposition solution without additives was prepared by mixing 80 ml of (Ethaline 200) with 0.7 mol L⁻¹ MnCl₂·4H₂O at 80°C to obtain a yellow-green transparent homogenous solution.

B) 0.05 mol L⁻¹ and 0.1 mol L⁻¹ of KBr were individually added to the Mn electrodeposition bath

2.4 Electrodeposition processes

2.4.1 Electrodeposition of Sn

Sn electrodeposition from 0.1 mol L⁻¹ SnCl₂·2H₂O in (Ethaline 200) solution was achieved on copper, brass, and on mild steel substrates, where the copper and brass cathode were cleaned by mechanical polishing, immersed in ammonium persulphate (NH₄)₂S₂O₈ solution, washed in water, and thereafter dried with acetone. The mild steel substrate was cleaned initially by mechanical polishing, washing with D.W, placing in conc. HCl acid, again washing in water, and next with acetone. The electrodepositions were performed at current density of 30 mA/cm². All experiments were carried out for 30 minutes.

2.4.2 Electrodeposition of Ag

As mentioned above, the copper, brass, and mild steel substrates were prepared to be employed as cathodes in an Ag electrodeposition process. At a fixed temperature of 80 °C and current density of 10 mA/cm² for 30 minutes, and using titanium mesh as the anode, the electrodeposition of Ag was achieved. [4]

2.4.3 Electrodeposition of Mn

Electrodeposition of Mn with and without addition of KBr was performed using the copper substrate. During the Mn electrodeposition processes, the temperature was fixed at 90°C. Mn was electrodeposited from Ethaline 200 containing 0.7 M $\text{MnCl}_2 \cdot 4\text{H}_2\text{O}$ under potentiostatic conditions by applying -1.75 V for 6 hours.

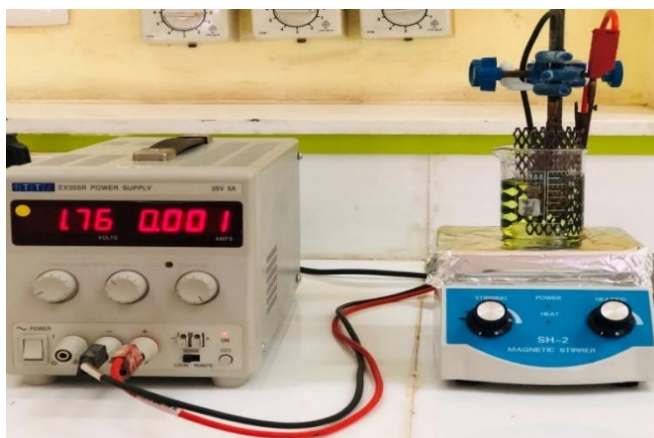
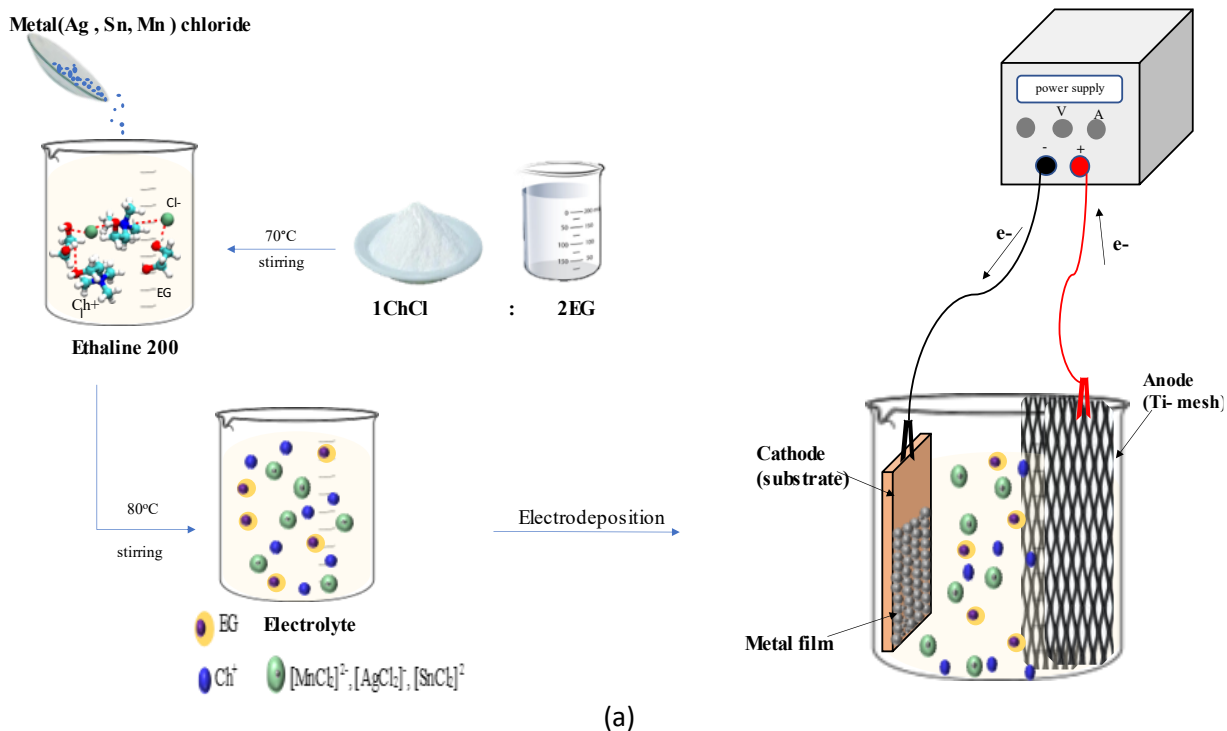


Figure 2. 1: (a) the schematic diagram of Electrodeposition steps of (Ag/Sn/Mn) (b) electrodeposition apparatus

2.5 Measurement of physical properties

2.5.1 Measurement of conductivity

Conductivity meter (DDS-22C) device, with a cell constant of 0.978 cm^{-1} , was utilized to measure the electrical conductivities of Sn, Ag, and Mn solutions. Conductivities were measured at different temperatures in the range 25-90°C.



Figure 2. 2: Conductivity meter device

2.6 UV-Visible spectroscopy measurements

In order to determine what there were changes in the Mn electroplating solution when adding of KBr and whether formation of another complexes, UV-Vis spectroscopy was performed.

The solutions that were examined included:

0.7 mol L^{-1} of $\text{MnCl}_2 \cdot 4\text{H}_2\text{O}$

0.7 mol L^{-1} of $\text{MnCl}_2 \cdot 4\text{H}_2\text{O}$ + 0.05 M KBr

0.7 mol L^{-1} of $\text{MnCl}_2 \cdot 4\text{H}_2\text{O}$ + 0.1 mol L^{-1} KBr

2.7 Electrochemical measurements

2.7.1 Cyclic voltammetry

Cyclic voltammetry is an electrochemical analytical technique for the study of redox reactions. It is used principally as qualitative analysis method by determining the formal oxidation and reduction potentials of chemical species in solution. It is also providing quantitative information about the analyte. Where the peak current provides information of about the concentration of analyte. Basic principle of CV is a triangular potential waveform is applied on the electrochemical system and the resulting current is measured. A plot of the current on y-axis versus potential on a x-axis is called cyclic voltammogram. [74]

The cyclic voltammetry experiments were performed via a PGSTAT20 potentiostat, in a three-electrode system consisting of a platinum working electrode, a platinum counter electrode, and an Ag reference electrode. The cyclic voltammetry of Sn was achieved over a potential range of 0.2 V to -1 V, whilst the potential window of silver was 0.3 to -0.3 V, and the cyclic voltammetry of Mn electrolyte with and without addition of KBr was examined in a potential range of 1.2 to - 1.8 V. All CV experiments were performed at varying temperatures (30, 50, 80°C) and scan rates (10, 20, 30, 40, 50, 60 mV/sec). The platinum working electrode was polished with alumina paste prior to each experiment.

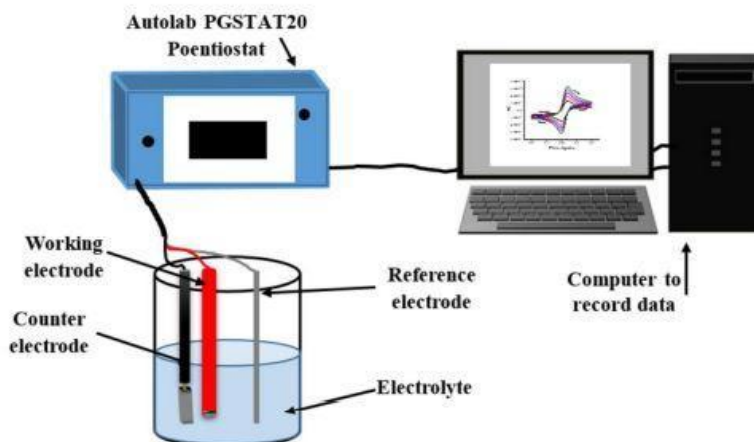


Figure 2. 3: Schematic diagram showing cyclic voltammetry system [21]

2.8 Surface analysis

2.8.1 Scanning electron microscopy and energy dispersive X-ray analysis (SEM/EDX)

Scanning electron microscopy is available to record fine detail images of the surface of matter. SEM utilizes the interaction between a focused beam of electrons with matter to produce a topological image, where such a beam will produce secondary electrons on interaction. EDX spectroscopy is the detection of the elemental composition of matter using scanning electron microscopy. [75]

The surface morphology of Sn, Ag, and Mn films was characterized using a TESCAN (MIRA 3) instrument with an accelerator voltage of 25.0 kV.

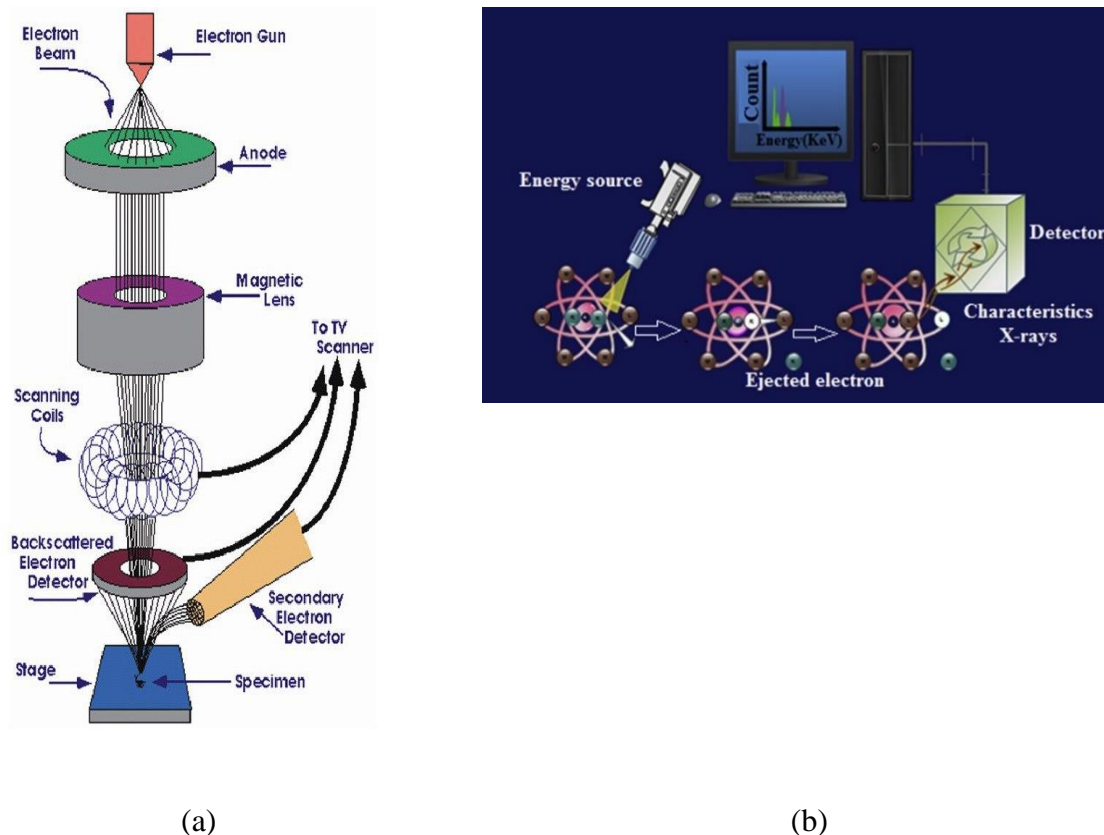


Figure 2. 4: a) Schematic diagram of the scanning electron microscopy (SEM) principle, b) Energy dispersive X-ray spectroscopy principle [76]

2.8.2 Atomic force microscopy

Atomic Force Microscopy is an excellent technique which provide roughness, topography, adhesion, and mechanical characterization of a broad range of materials. The basic principle of AFM can be summarized by noting that the tip of the apparatus moves via piezoelectric (PZT) over the surface of sample, then the force (F) between the tip and the surface can be measured via a force transducer, and a feedback control supplies the signal from the force transducer to piezoelectric in order to keep the force fixed between the sample and tip [77], as shown in **Fig. 2.5**.

Atomic force microscopy was conducted using a NTEGRA (NT-MDT) instrument in non-contact mode to determine the 3D surface morphology of the Ag, Sn, and Mn deposits and to measure the roughness of the films.

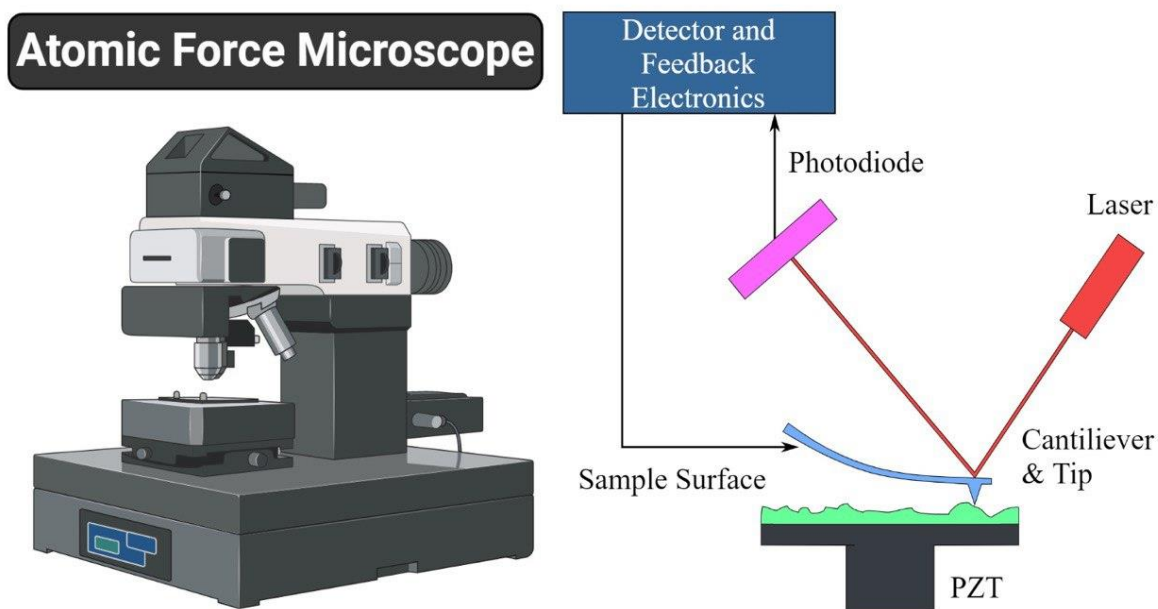


Figure 2. 5: An illustration of the AFM instrument and a schematic diagram illustrating the principle of atomic force microscopy

2.8.3 X-ray diffraction

The principle of the X-ray diffraction technique is dependent on the constructive interference of monochromatic X-rays with crystalline matter. The incident X-ray interacts with the sample and produces constructive interference and diffracted rays only under those conditions that obey Bragg's law: $n\lambda = 2d\sin\theta$, where n is an integer, λ is the wavelength of the X-rays, d is the interplanar spacing generating the diffraction, and θ is the diffraction angle. These diffracted X-rays are then detected, processed, and counted [78].

Powder X-ray diffraction was achieved via an Philips (PW1730) instrument. The Cu anode was used as X-ray tube with 1 deg, 1deg and a 0.2 mm slit monochromator-filtered radiation wave. It was carried on at 40 kV and 30 mA.

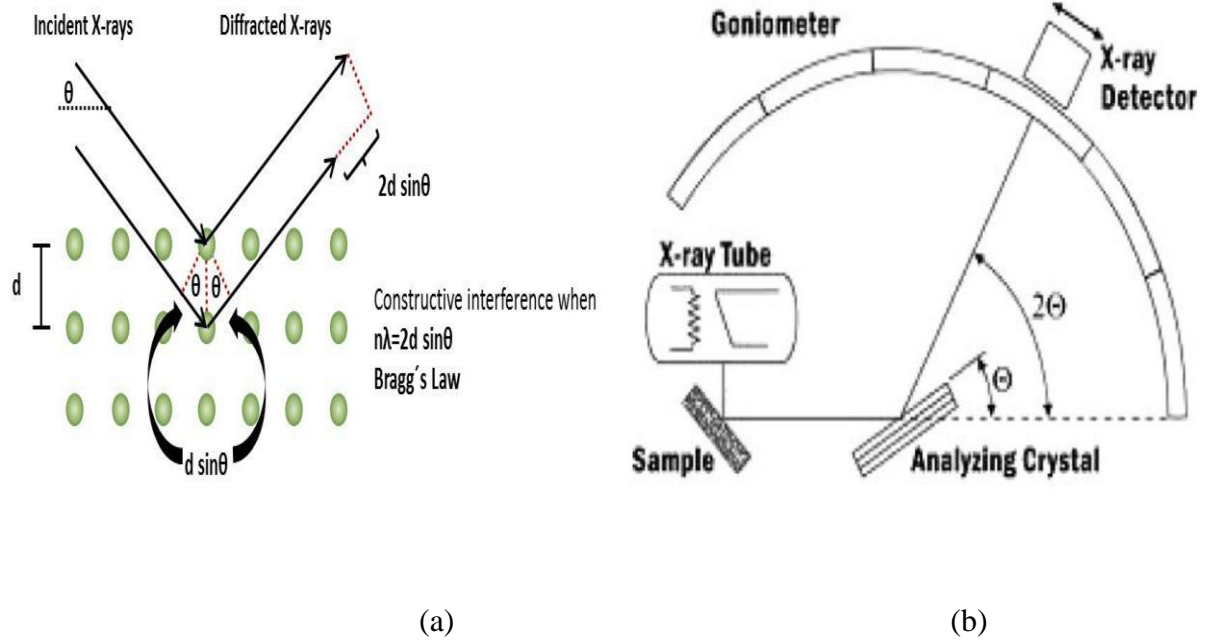


Figure 2. 6: a) Schematic diagram of X-ray diffraction, b) schematic diagram of a diffractometer.

Chapter Three
Results and Discussion

Chapter three: Results and discussion

3.1 Tin electrodeposition

3.1.1 Physical Properties

Most electrodeposition from ILs investigations yet have paid little interest to how adding boric acid affects the physical characteristics of Ethaline 200. Viscosity has a direct impact on the rate of movement of the reactive ingredient to the electrode surface for deposition, which in turn affects coating rate. In this work, we demonstrate that boric acid has an obvious effect on the viscosity and conductivity of the DES Ethaline 200. Moreover, viscosity is a key characteristic of ionic liquids which are used as dissolvents and electrolyte solutions. This physical property of ionic liquids is acquired by van der Waals forces and hydrogen bonding [79]. The viscosity of $\text{SnCl}_2 \cdot 2\text{H}_2\text{O}$ in 1ChCl:2EG is described in **Fig. 3.1 (a)** as a function of temperature and various boric acid concentrations. As can be observed, boric acid has no appreciable impact on a substance's capacity to flow and very slightly raises the viscosity of the $\text{SnCl}_2 \cdot 2\text{H}_2\text{O}$ in a 1:2 ChCl:EG solution. The establishment of large numbers of hydrogen bonds typically results in an increment in the viscosity of the associated ionic liquid. This might be caused by the liquid disrupting the lattice and changing the coordination of the Cl^- dialogue.

The corresponding change in conductivity with respect to the presence of different concentration of boric acid in 1:2 ChCl: EG is shown **Fig. 3.1(b)**. Here, the conductivity is presented in an analogous manner to the viscosity and decreases as a function of the concentration of boric acid. **Fig. 3.1(b)** depicts the conductivity of $\text{SnCl}_2 \cdot 2\text{H}_2\text{O}$ in 1:2 ChCl:EG as a function of temperature and different amounts of boric acid. As a consequence, the conductivity with different concentrations of boric acid shows a differing pattern to that of the viscosity, as the conductivity of the metal salt solution decreases significantly with increasing concentration of boric acid. As a result, this compound more probably exhibit inhibition conductivity of $\text{SnCl}_2 \cdot 2\text{H}_2\text{O}$ in Ethaline 200. It has also been shown in **Fig. 3.1(b)** that the conductivity of $\text{SnCl}_2 \cdot 2\text{H}_2\text{O}$ with different concentrations of boric acid increases significantly with increasing temperature.

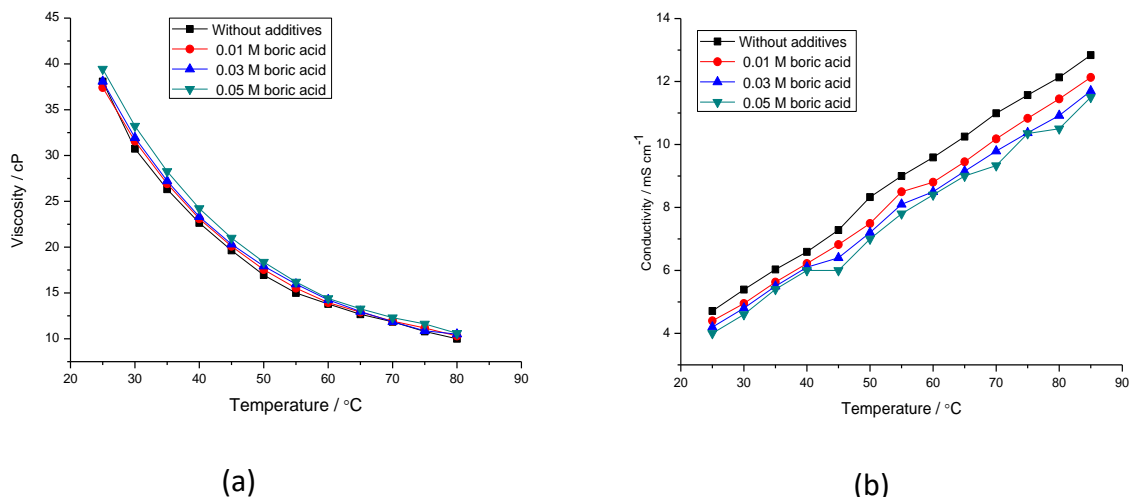


Figure 3. 1: (a) The viscosity (b) The conductivity of 0.1 mol L⁻¹ SnCl₂·2H₂O in Ethaline 200, at a range of temperature (25-90 °C) and various amounts of BA

3.1.2. Cyclic voltammetry

Fig. 3.2 indicates the cyclic voltammograms of 0.1 mol L⁻¹ SnCl₂·2H₂O in Ethaline, where the voltammograms were undertaken using a Pt disc (WE), a Pt flag (CE), and Ag wire (RE). The cyclic voltammetry was achieved starting from 0.2 V and cycling in the negative path, ending at -1 V, and then reversing again to 0.2 V. The cyclic voltammetry of 0.1 mol L⁻¹ SnCl₂·2H₂O at different temperatures was investigated, as shown in **Fig. 3.2 (a)**, where increasing cathodic and anodic peak intensities were observed with increasing temperature. Elevated temperature increases the free volumes in IL., increasing the mass transport towards the electrode surface as a result of the decrease in viscosity and increase in the movement of ions, which then accelerates the oxidation-reduction processes. **Fig. 3.2 (b)** shows the cyclic voltammograms performed at different scan rates at 80°C. It is apparent from these latter voltammograms that appearing two reduction peaks relating to the reversible Sn²⁺ to Sn⁰ couple at -0.4 V, while the stripping peak at -0.3 V is related to Sn dissolution (from Sn⁰ to Sn²⁺). Here, the scan rate has no observable effect on the cathodic and anodic peaks. **Fig. 3.2 (c)** shows the comparison between the cyclic voltammograms of a solution of 0.1 mol L⁻¹ SnCl₂·2H₂O at 80°C in the free additive electrolyte and contain of different concentrations of boric acid. **Fig. 3.2 (c)**. There is a little decrease in the Sn deposition peak, which occurs at negative potential, in the presence of BA. this is due to

the adsorption of BA onto the surface of electrode, hindering Sn deposition. Moreover, a negative shift in the Sn reduction potential recorded as BA was inserted into the Sn electrolyte, which can again be attributed to the adsorption of BA onto the electrode surface, thus requiring additional energy to discharge the Sn ions.

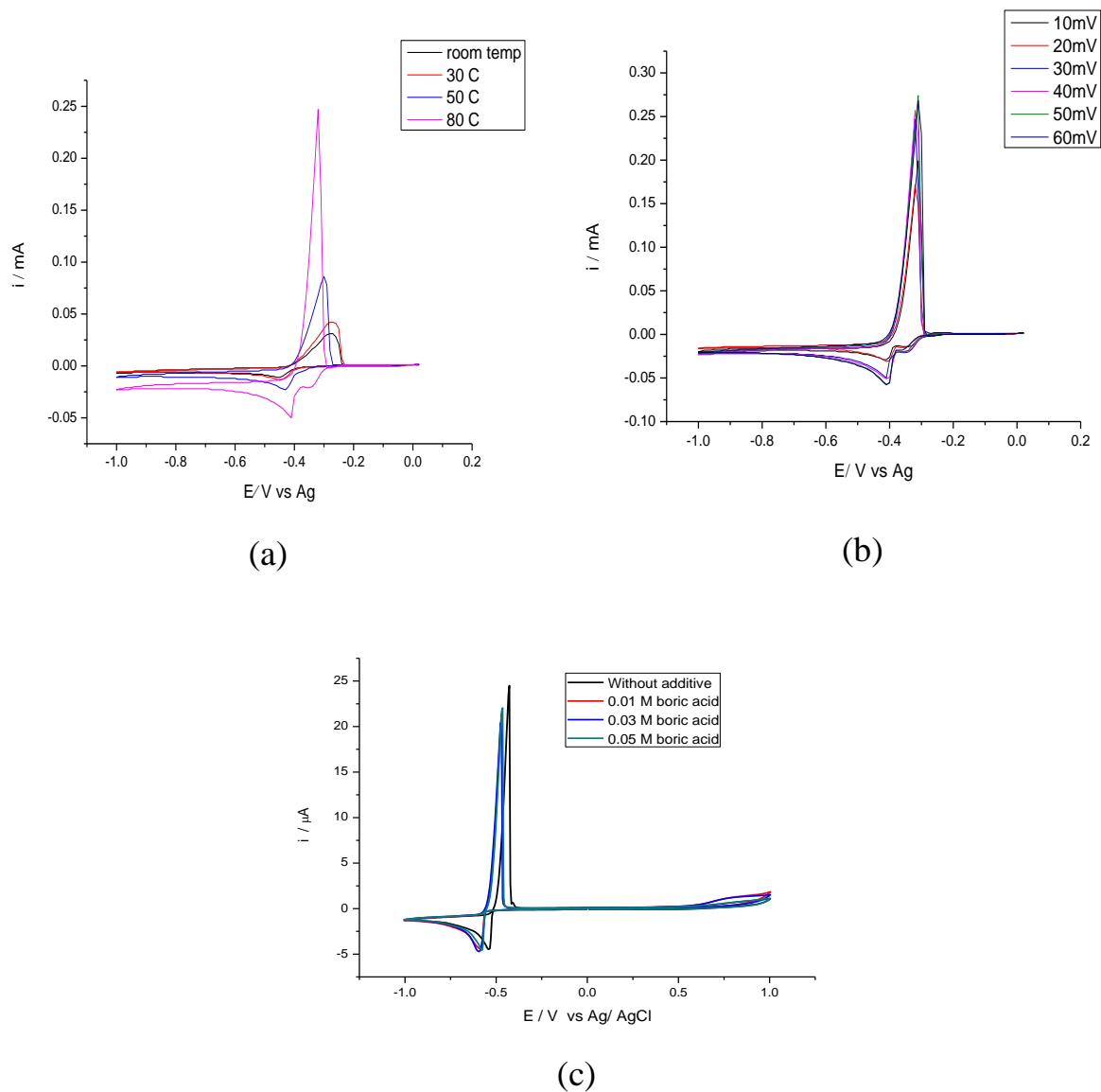


Figure 3. 2: Cyclic voltammograms of $0.1 \text{ mol L}^{-1} \text{ SnCl}_2 \cdot 2\text{H}_2\text{O}$ in Ethaline 200: a) different temperatures at a scan rate of 30 mV s^{-1} , b) different scan rates, and c) different concentrations of boric acid. All depositions were achieved using a Pt disc (working electrode), a Pt flag (counter-electrode), and Ag and Ag/AgCl (reference electrode).

3.1.3. surface analysis

3.1.3.1 Effect of temperature on the electrodeposition of Sn

In this work, to study the effect of temperature on the morphology of Sn deposit, the electrodeposition process was achieved at low (room) temperature and at high (80°C) temperature, as shown in **Fig. 3.3**, where both films were deposited on a copper substrate at 30 mA cm⁻² for 30 min. A dark-colored and heterogenous film was observed when electrodeposition was performed at room temperature, as illustrated in **Fig. 3.3 (a)**, in comparison with that performed at 80°C, where a bright and uniform Sn coating was instead formed. As shown above, the temperature has a significant impact on the conductivity, as per **Fig. 3.1**, and on the cyclic voltammetry of the electrolyte during Sn deposition, **Fig. 3.2 (a)**, and thus has an effect on the morphology of the Sn film so deposited. At high temperature, the Cl⁻ anion concentration decreases, which allows Sn deposition to proceed at a high rate and thus with high current efficiency [71]. As well as the rise temperatures might enhance mass transport impacts through the resultant decrease in the viscosity of the Sn electrolyte. accordingly, from cyclic voltammetry and morphological figures, the electrodeposition of Sn from Ethaline 200 at high temperature is required for the production of a uniform and bright Sn deposition. and as a result, in this work, the electrodeposition of Sn from Ethaline 200 in the absence and presence of boric acid has been done at 80°C.

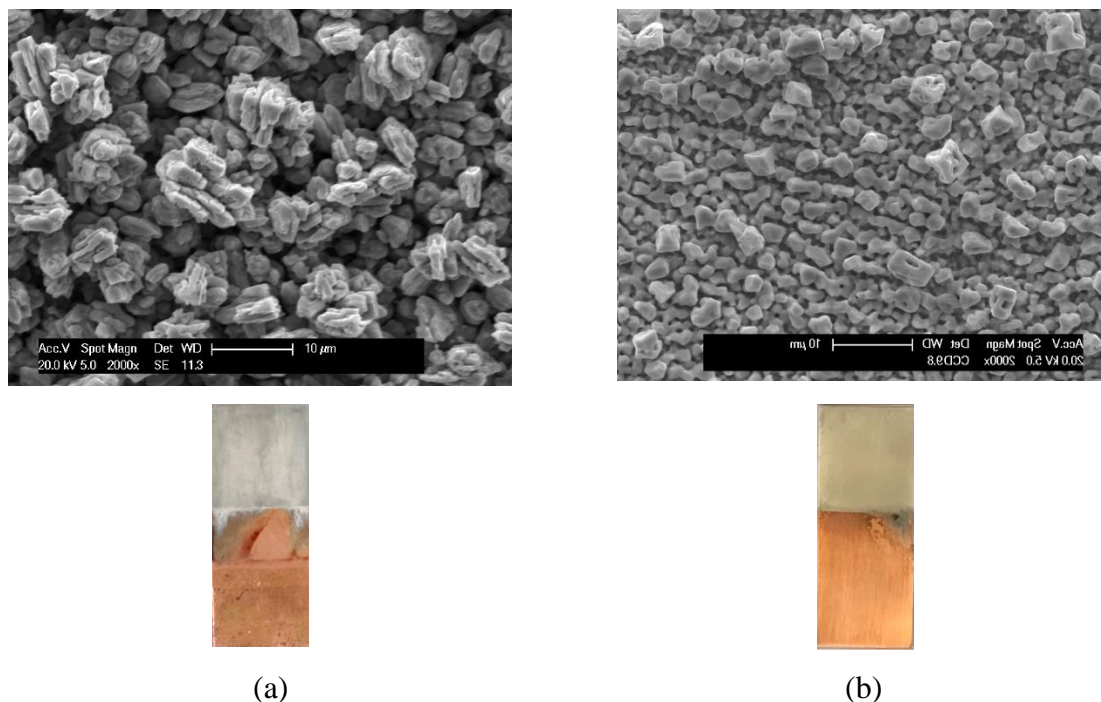


Figure 3. 3: SEM images for Sn electrodeposited from $0.1 \text{ mol L}^{-1} \text{ SnCl}_2 \cdot 2\text{H}_2\text{O}$ in Ethaline 200. Both films were performed on a copper substrate and at a current density of 30 mA cm^{-2} , a) at room temperature, b) at 80°C .

3.1.3.2. Effects of boric acid on the electrodeposition of Sn

Fig. 3.4 shows the optical photographs, SEM morphologies, and AFM images for Sn electrodeposition in presence/absence of various concentrations of BA in a Ethaline 200 containing $0.1 \text{ M SnCl}_2 \cdot 2\text{H}_2\text{O}$ electrolyte at a determined bath temperature of 80°C . In all experiments, the current density was fixed at 30 mA cm^{-2} , and electroplating was implemented for 30 minutes on Cu substrates. In fact, good adherence was achieved for all Sn coatings using boric acid. In the electrodeposited additive-free Sn film, the morphology of the film was found to be that of a rough layer with larger grains, as shown in the inset of **Fig. 3.4 (a)**. However, we note that the surface morphologies of the Sn deposits change with the addition of the BA additive to the Sn plating bath **Fig. 3.4 (b), (c), and (d)**. Obviously, the sizes of particles were considerably reduced, and the particle grains progressively became littler with increasing amounts of BA additive in the electrolytes; the surface morphology became higher smooth and homogeneous with concentration in comparison to the Sn deposition from free

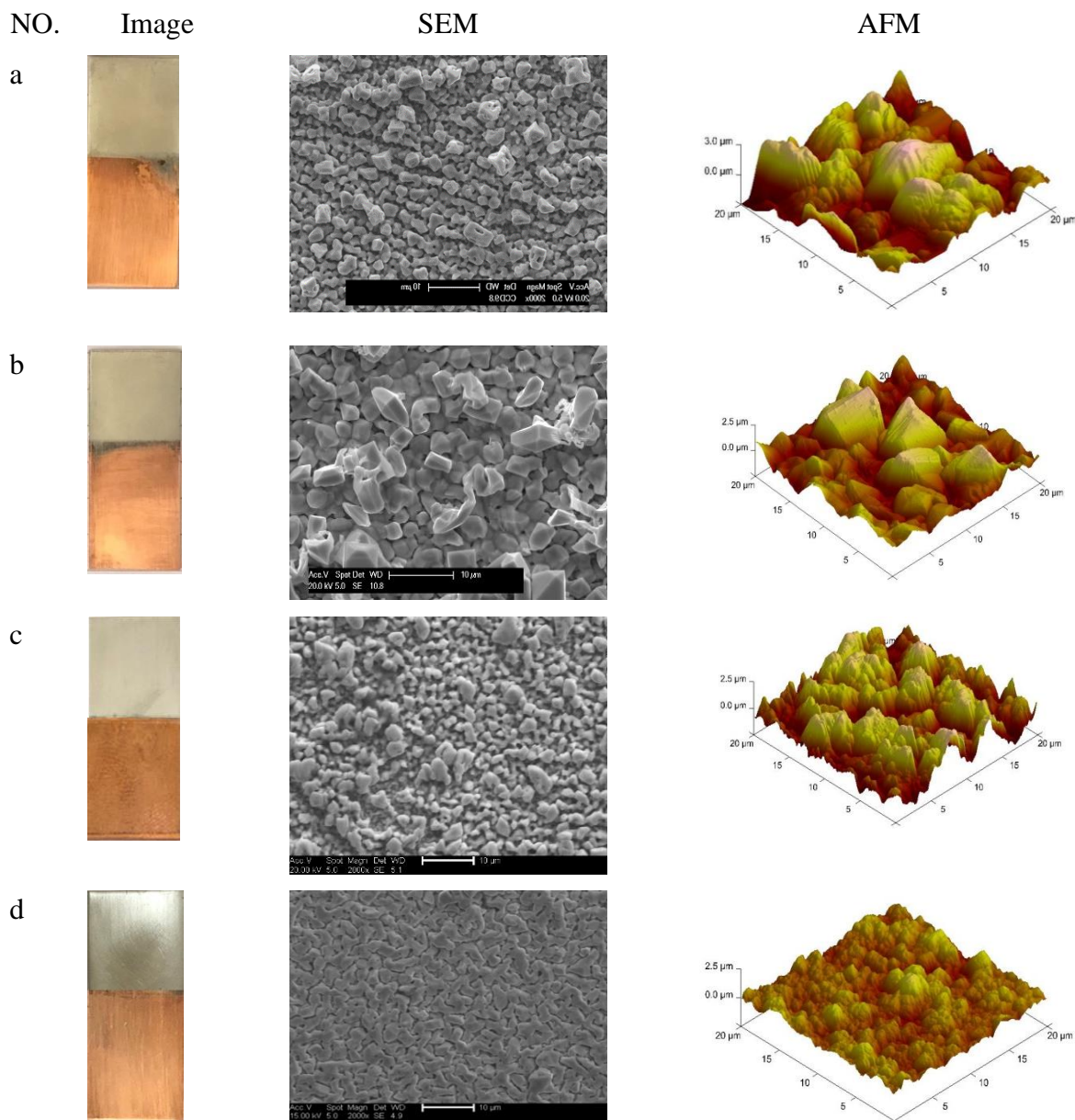


Figure 3. 4: Visual photos, SEM morphologies, and AFM from left to right respectively of Sn films obtained from Ethaline 200 containing $0.1 \text{ mol L}^{-1} \text{ SnCl}_2 \cdot 2\text{H}_2\text{O}$ with and without various amounts of BA for 30 min. on a Cu substrate at $80 \text{ }^\circ\text{C}$ at 30 mA cm^{-2} current density. Image a) is for the Sn deposition without BA, with b) 0.01 M BA, c) 0.03 M BA, and d) 0.05 mol L^{-1} BA

BA electrolyte. This is a result of the decreased crystal size due to the addition of [various concentrations of] BA. This suggests that BA may would lead to a reduction in growth rate of the Sn deposit.

AFM was utilized to study the topography and roughness of the tin deposits provided from Ethaline 200 on the copper in both the absence and presence of BA. AFM scans were performed over an area of $2.0 \times 2.0 \mu\text{m}$. **Table 3.1** shows average surface roughnesses of Sn films, where it is clear that the roughness of the Sn film reduced with increasing concentration of BA in the electrolyte.

Table 3. 1: Average surface roughnesses of Sn films

Metal salt	Conc. BA / M	Average roughness/ nm
SnCl ₂ .2H ₂ O	0.00	32.08
SnCl ₂ .2H ₂ O	0.01	20.9
SnCl ₂ .2H ₂ O	0.03	12.5
SnCl ₂ .2H ₂ O	0.05	7.9

3.1.3.3 Electrodeposition of Sn on different substrates

The morphologies of Sn deposits on copper, mild steel, and brass substrates were characterized via SEM, as shown in **Fig. 3.5**. The depositions were achieved at 80 °C for 30 minutes and at 30 mA cm⁻² current density in presence of 0.05 M BA. uniform and homogenous morphology, bright and small particle sizes for the Sn deposits were formed on the all these substrates and no noticeable effect of substrate on the morphology of the Sn films. The EDX spectra in **Fig. 3.5** confirm that the films are formed from Sn.

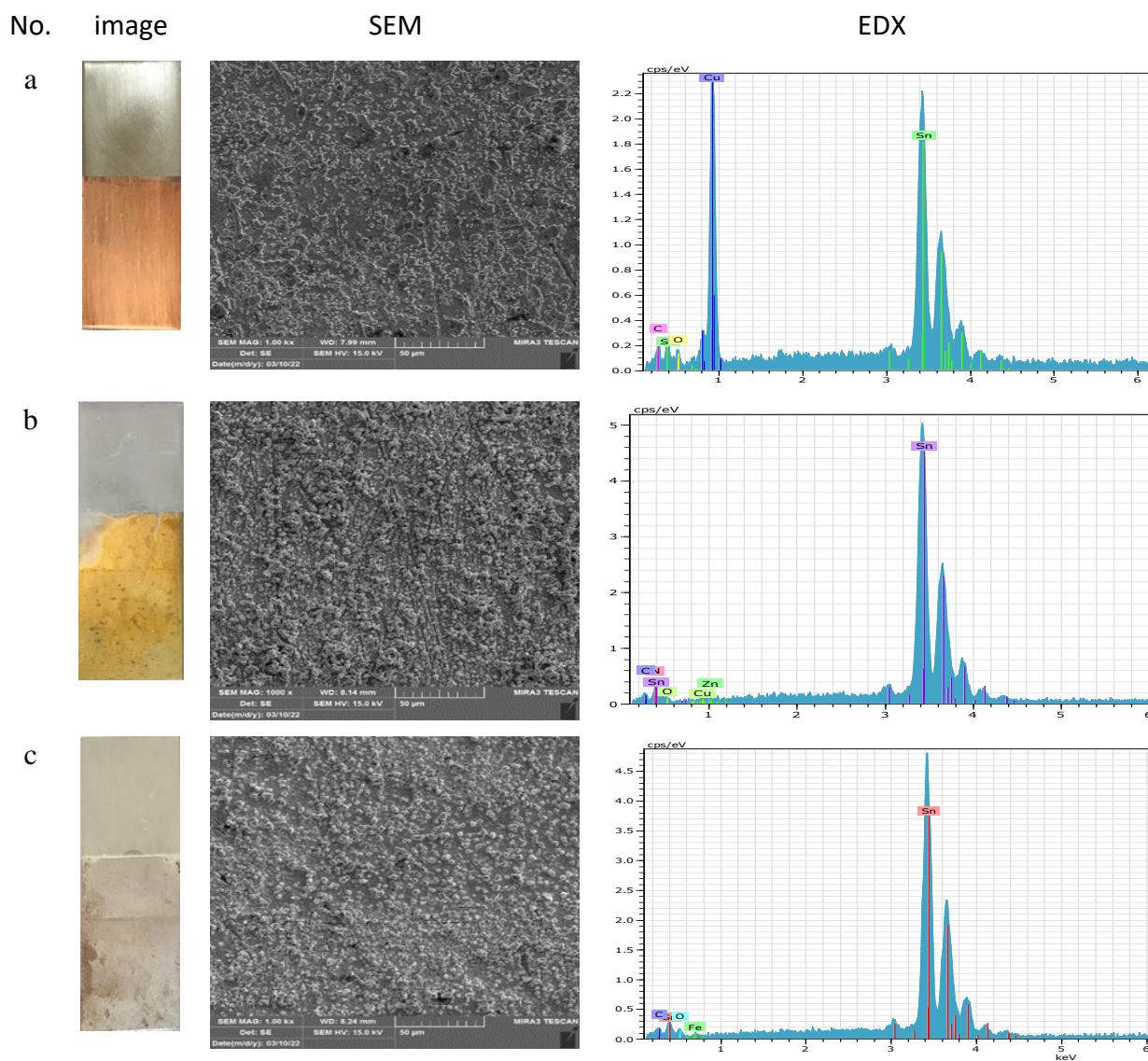


Figure 3. 5: SEM images and EDX spectra for the electroplating of $\text{SnCl}_2 \cdot 2\text{H}_2\text{O}$ (a) on a copper substrate, (b) on a brass substrate, and (c) on a mild steel substrate. All experiments were carried out at 80°C for 30 min.

In this work, the crystal structures of the Sn films electroplating from the Ethaline electrolyte on copper, brass, and mild steel substrates were studied via XRD. **Fig. 3.6** shows the XRD patterns for deposits of Sn. The (200), (101), (220), (211), (301), (112), (321), (420), and (312) planes related to Sn deposits were observed at 30.5° , 32° , 44.2° , 44.9° , 55.3° , 62.5° , 64.6° , 73.8° , and $79.5^\circ 2^\theta$ respectively

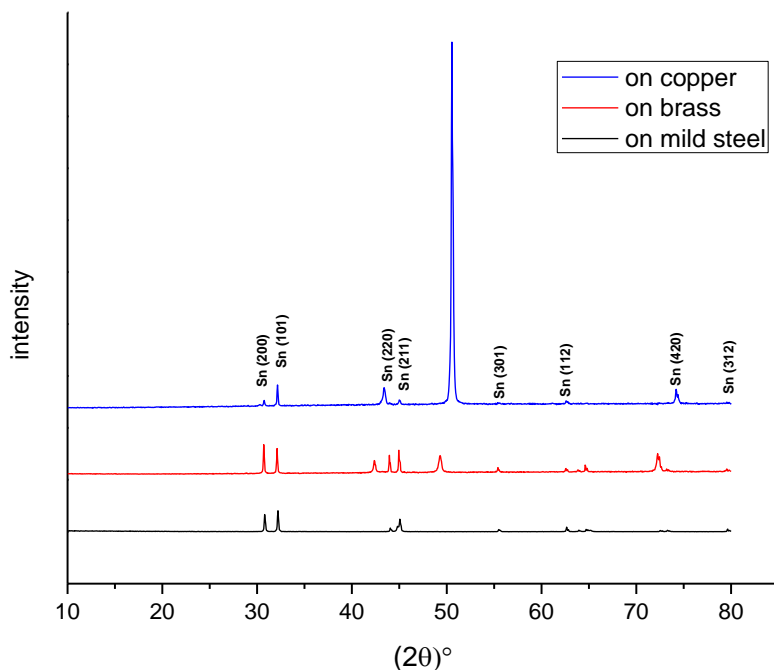


Figure 3. 6: XRD patterns for Sn films from 0.1 M $\text{SnCl}_2 \cdot 2\text{H}_2\text{O}$ in Ethaline on mild steel, brass, and copper electrodes. All experiments were carried out for 30 min. at 80°C and at a current density 30 mA cm^{-2}

3.2 silver electrodeposition

3.2.1 Conductivity

The conductivity of Ethaline 200 containing 0.05 M AgCl solution was measured as function of temperature (25-90°C). **Fig. 3.7** shows that the conductivity of the solution was significantly affected by temperature, where it decreases with decreasing temperature.

In general the ions of DESs have a large size in contrast to the voids between these ions. These voids represent the free space between the different portions ions/molecules, which formed the DESs, and are called holes. Hole theory is considered to be accurate model for study the conductivities of deep eutectic solvents and ionic liquids. In hole theory the principal assumption is that orientation and voids of random size are formed when solid is melt. The relative abundance of suitable sized holes and size of the ions are considered to be effected move ability of an ion. The mass transport properties of ILs have been measured using the hole theory and show a strong degree of correlation with experimentally obtained value. This correlation suggests that mass transport in deep eutectic solvents, which consist of asymmetric ions, is principally controlled by the availability of suitably sized holes. This is in contrast to the classical high temperature molten salts, which are in general contain a small symmetric ions, where mass transport is primarily controlled by the charge carriers concentration.[68]

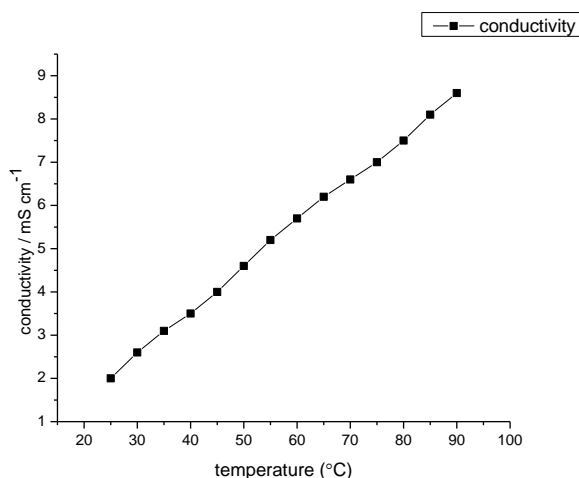


Figure 3. 7: Conductivity diagram of AgCl in Ethaline 200 different temperatures

3.2.2 Cyclic voltammetry

Cyclic voltammetry was examined to study the redox behavior of Ag in an Ethaline 200 (1:2 ChCl:EG mixture)-based DES. **Fig 3.8** points to cyclic voltammograms of 0.05 mol L⁻¹ AgCl in Ethaline 200. All these voltammograms were carried out employing a working-electrode (Pt disc), a counter-electrode (Pt flag), and reference electrode (Ag wire). The potential window used was from 0.3 to -0.3 V. The experiments were individually run at different temperatures and different scan rates. **Fig 3.8 (a)** displays the cyclic voltammograms of 0.05 M AgCl in Ethaline 200 at 80°C and at various scan rates (10, 20, 30, 40, and 50 mVs⁻¹). Here, the Ag cathodic reduction peak was observed at about -0.05 V and the anodic stripping peak at about +0.06 V.

As can be explain in **Fig 3.8 (b)**, there are notable changes in the intensities of the Ag oxidation and reduction peaks at high temperature (80°C) compared with those measured at lower temperatures. The increase in the intensity of redox peaks for this Ag system when cyclic voltammetry was measured at elevated temperature might be since the increase in the free volumes in the solution, decreased viscosity, and decrease in the number of Cl⁻ anions adsorbed on the electrode, which would lead to an increase in the rates of any oxidation-reduction processes.

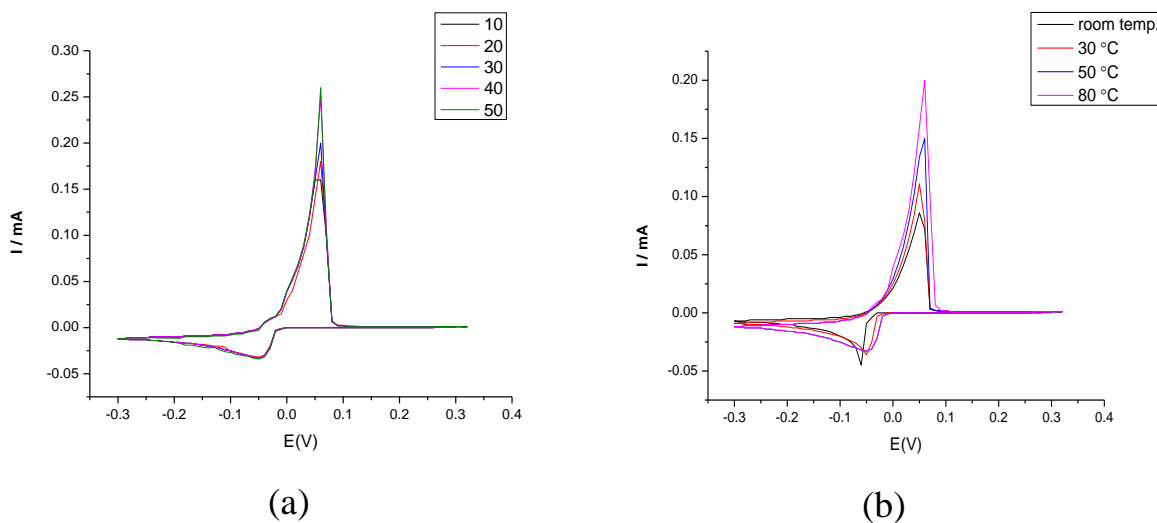


Figure 3. 8: Cyclic voltammograms of 0.05 M AgCl in Ethaline 200 on a Pt disc electrode (a) at different scan rates, (b) at different temperature

3.2.3 Surface analysis

Fig 3.9 shows the optical images, micrographs, and EDX spectra for the Ag deposit from Ethaline 200 containing 0.05 M AgCl on copper, brass, and mild steel substrates. The SEM for silver deposited on copper appeared to show accumulations of small spherical particles. The Ag on brass substrate was found to have a porous surface with a dendritic shape-type structure, while the deposit on the mild steel substrate showed a change in morphology, where in this latter case separated particles were distributed along the substrate. The chemical analysis of the Ag films, as carried out via EDX, reveals the presence of Ag in all samples.

The electrodeposition of Ag from Ethaline 200 is strongly affected by the substrate material. For copper and copper alloy substrate was formed compared to mild steel substrate this may be due to the varying in reduction potential between Ag and Cu.

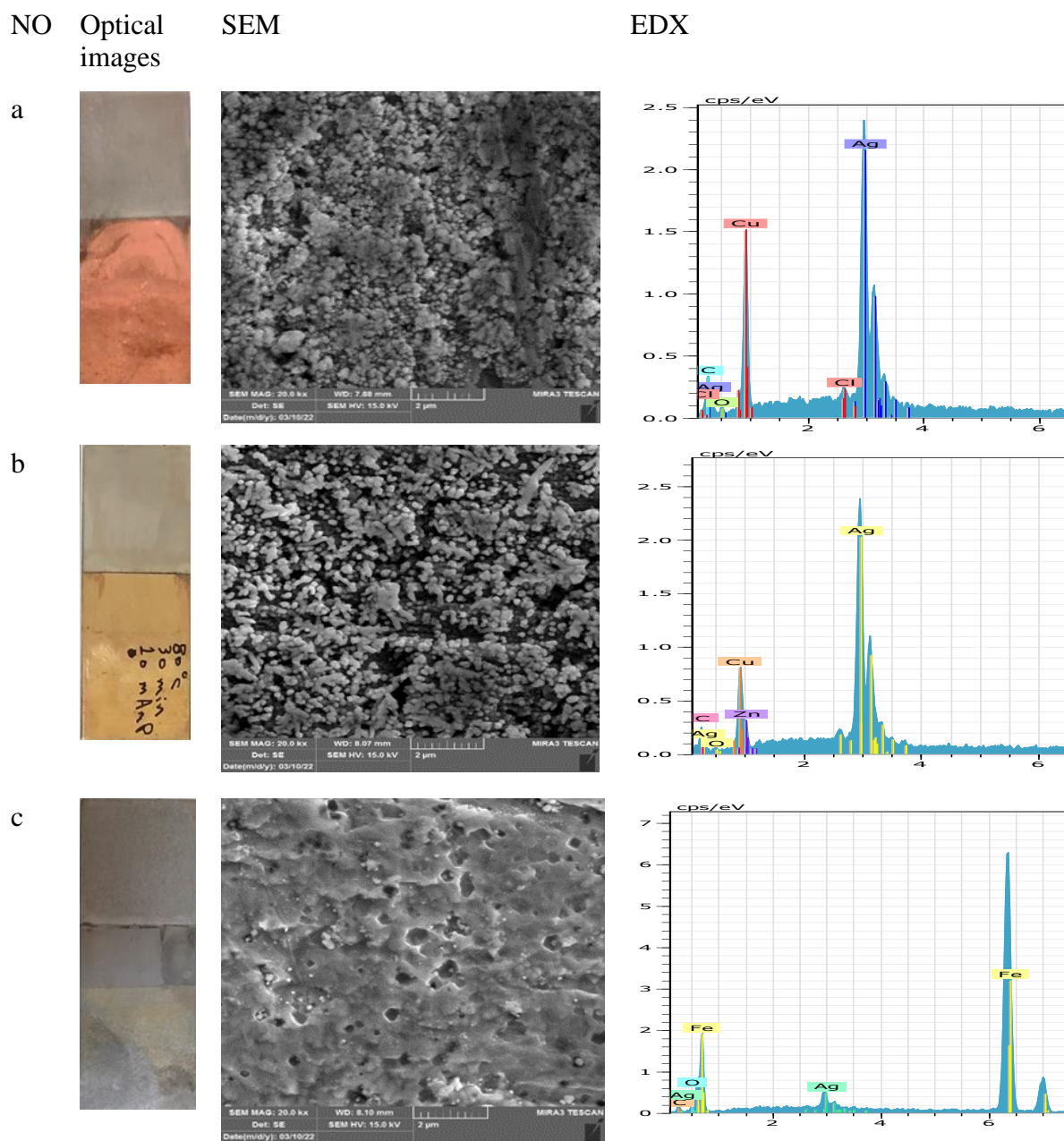


Figure 3. 9: Optical image (left), SEM images (middle), and EDX spectra (right) of Ag films obtained on (a) copper, (b)brass, and (c) mild steel substrates.

Atomic Force Microscopy is a very high-resolution form of scanning probe microscopy (SPM). It is an excellent technique for provides roughness, topography, adhesion, nucleation, and mechanical characterization of a broad range of materials. This technique can be used to study the structure of conducting and isolating surfaces in air environments as well as liquid. Atomic force microscopy (AFM) was used to study the topographies and roughness of the Ag deposited on the surfaces. **Fig. 3.10** shows the AFM images of an Ag deposit from Ethaline 200 at 80°C on copper, brass, and mild steel substrates at a current density of 10 mA cm⁻² for 30 min. in each case. The results of the AFM analysis were in good agreement with those obtained from SEM.

The average roughness of each of the Ag films was also measured via AFM. **Table 3.2** reports the average roughness of the Ag films produced from Ethaline 200 on different substrates, where a smoother Ag film was obtained when the electrodeposition was carried out on the copper substrate.

Table 3. 2: Average surface roughness of various Ag films

Metal salt	Substrate	Average roughness, nm
AgCl	mild steel	27
AgCl	brass	25
AgCl	copper	6

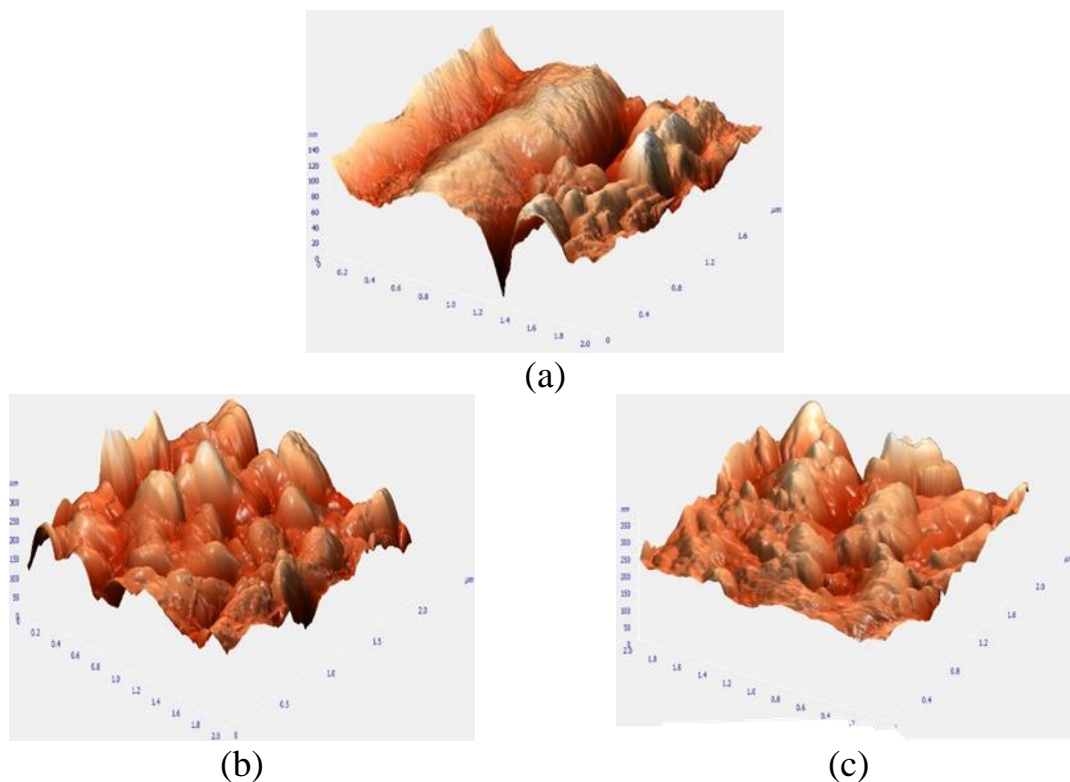


Figure 3.10: AFM images of Ag films electrodeposited on different metallic substrates: (a) on copper, (b) on brass, and (c) on mild steel

The crystal structure of the Ag deposited upon different metallic substrates (copper, brass, and mild steel) at 80 °C and 10 mA cm⁻¹ for 30 min. was verified via XRD. The X-ray diffractograms of these Ag films are given in **Fig 3.11**. The diffraction peaks recorded at 38.1°, 44.3°, 64.5°, and 77.4° are correlated well with the JCPDs card of Ag (JCPDs file no.065-7244) [80]. The X-ray diffractograms of Ag deposits procceed on copper and brass substrates appeared diffraction peaks at 43.35°, 50.49°, and 74.19° Bragg angles, indicating that there was Cu in the substrate.

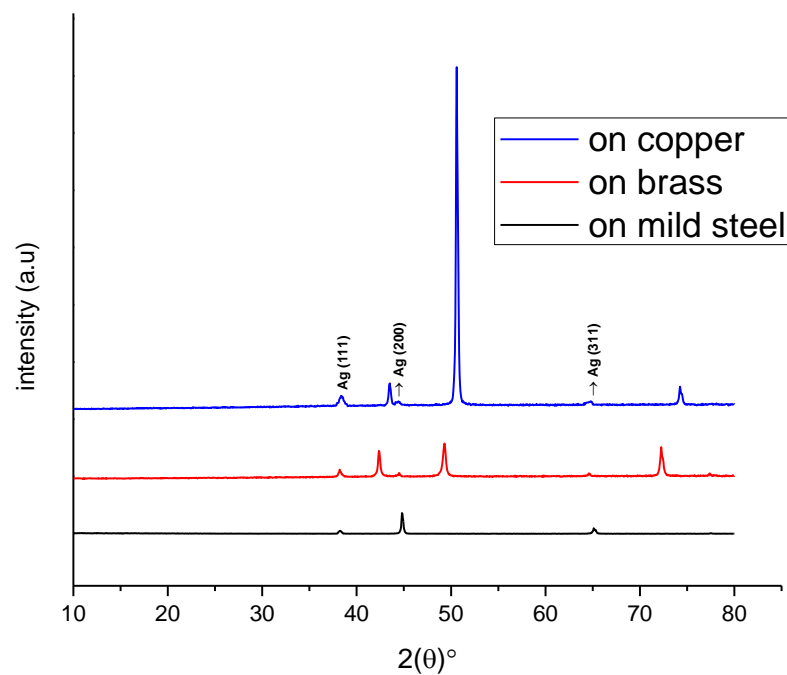


Figure 3. 11: X-ray diffractograms of Ag films deposited from Ethaline 200 at 80 °C, 10 mA cm⁻¹ current density, on different substrates copper, brass, and mild steel

3.3 Manganese electrodeposition

3.3.1 Speciation

Speciation is known to control key aspects of electrochemical behavior (such as redox potentials and solubility) and metal processing. In aqueous solution, highly toxic reagents, such as cyanide, commonly have to be used to give metal ions the needed redox properties, because of domination of the speciation by aquo-complexes, whereas in ILs and DESs there is some proof that speciation is controlled by the anionic component of the liquid

UV-vis spectroscopy was employed to study the speciation of $\text{MnCl}_2 \cdot 4\text{H}_2\text{O}$ in Ethaline 200 in the absence and presence of different concentrations of KBr. **Fig.3.12 (a)** shows the appearance of 0.7 M of $\text{MnCl}_2 \cdot 4\text{H}_2\text{O}$ with and without 0.05 M and 0.1 M KBr. The color of the $\text{MnCl}_2 \cdot 4\text{H}_2\text{O}$ in Ethaline 200 without KBr was yellow- green, which implies the presence of $[\text{MnCl}_4]^{2-}$ complexes[81]. A change of color from yellow- green to green was observed when adding KBr. The intensity of the associated bands increases with increasing concentration of KBr, as shown in **Fig. 3.12 (b)**. From **Fig. 3.12 (b)** it can be seen that there was no remarkable change in the absorption spectra of Mn when adding KBr this indicate that KBr does not complex with the Mn species present in Ethaline 200.

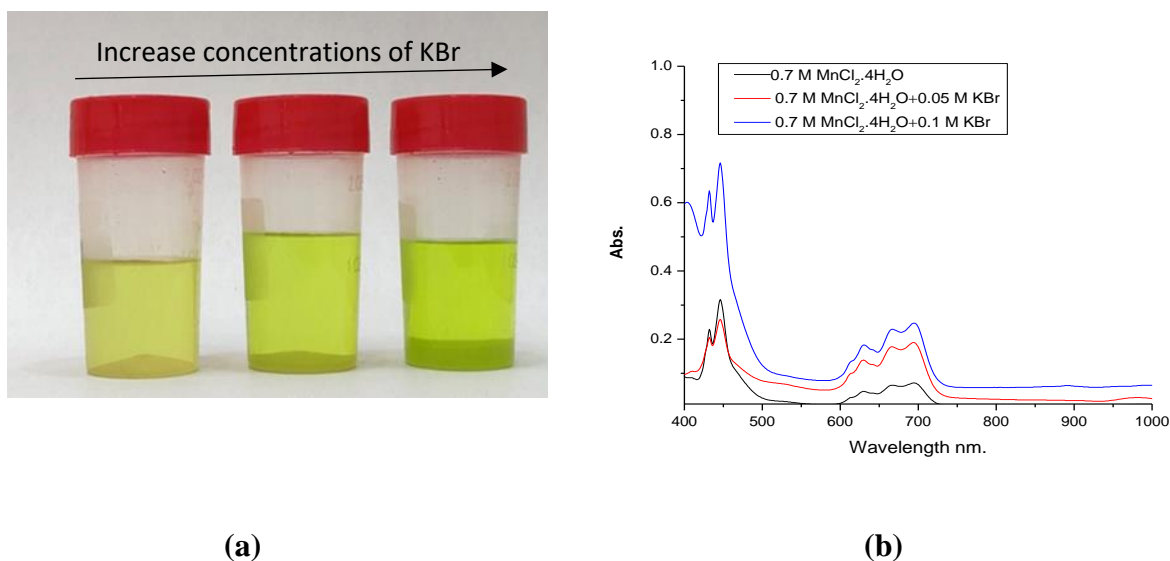


Figure 3. 12: (a) optical image of 0.7 M $\text{MnCl}_2 \cdot 4\text{H}_2\text{O}$ in Ethaline 200 containing different concentrations of KBr, (b) UV-vis spectra for 0.7 M $\text{MnCl}_2 \cdot 4\text{H}_2\text{O}$ in Ethaline 200 with different concentrations of KBr

3.3.2 Conductivity

The impact of different concentrations of KBr on the conductivity of Ethaline 200 containing 0.7 M of $\text{MnCl}_2 \cdot 4\text{H}_2\text{O}$ at temperatures in the range 25-90°C were investigated, as shown in **Fig. 3.13**. Here, a decrease in the conductivity of Mn solution in the presence of KBr was observed, which may be due to the KBr increasing the viscosity of solution.

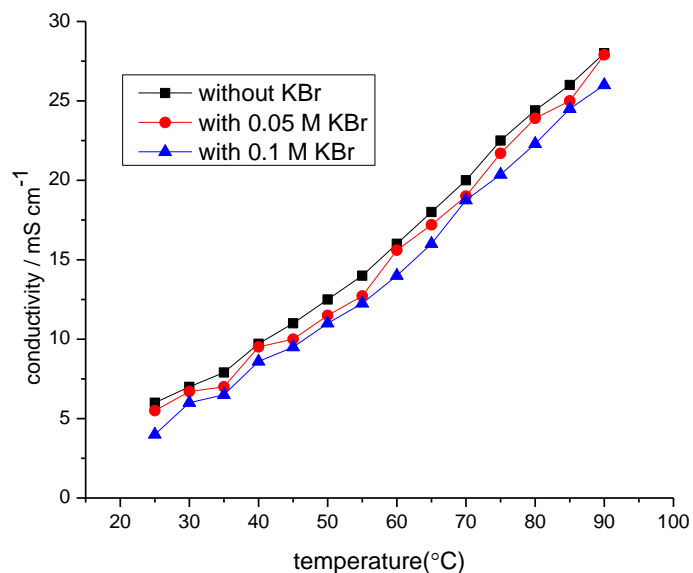


Figure 3. 13: Conductivity of 0.7 M $\text{MnCl}_2 \cdot 4\text{H}_2\text{O}$ in Ethaline 200 with different concentrations of KBr as a function of temperature

3.3.3 Cyclic voltammetry

Cyclic voltammetry was performed to exam the electrochemical behaviors of pure Mn with different amounts of KBr in Ethaline solution. The cyclic voltammograms obtained from Ethaline containing 0.7 mol L⁻¹ MnCl₂.4H₂O solution at 80°C on a platinum electrode, measured at different scan rates, are shown in **Fig. 3.14 (a)** in the voltammogram of 0.7 mol L⁻¹ MnCl₂.4H₂O in Ethaline 200, where the reduction of Mn species started at about -1.5 V on the Pt electrode, while no clear oxidation peak for Mn was found. There is a certain similarity between the present voltammograms of Mn in Ethaline and those described by Pereira et al. [82], who noted that the absence of an oxidation peak in the CV of Mn may have been due to the instability of the Mn deposits, which readily oxidized in the electrolyte.

Fig. 3.14 (b) shows cyclic voltammograms of 0.7 M MnCl₂.4H₂O in Ethaline 200 with and without of 0.05 mol L⁻¹ and 0.1 mol L⁻¹ KBr at 80°C. In the solution containing 0.1 mol L⁻¹ KBr two oxidation peaks can be seen first peak was indicate to oxidation of bromide to tribromide **Equation (3-1)** and second peak was indicate to oxidation of tribromide to bromine. [83]



increases in the reduction current peak of Mn species have been observed when the C.V. process was recorded using electrolytes with KBr. This was anticipate for two reasons: firstly, due to the reduction of both tribromide and Mn²⁺ to Mn at nearly same potential. Secondly, Br₃⁻, which produced from addition of KBr to the Mn electrolyte, may be adsorbed as monolayer on the surface of electrode, leading to an increase in the deposition rate and then improvement the Mn electrodeposition by prevent the formation of Mn oxide passivation layer on the electrode surface, the reduce of the effects of passivation layer is considered as one reasons for increase the intensity of reduction peak of Mn in Ethaline 200 in presence of KBr.

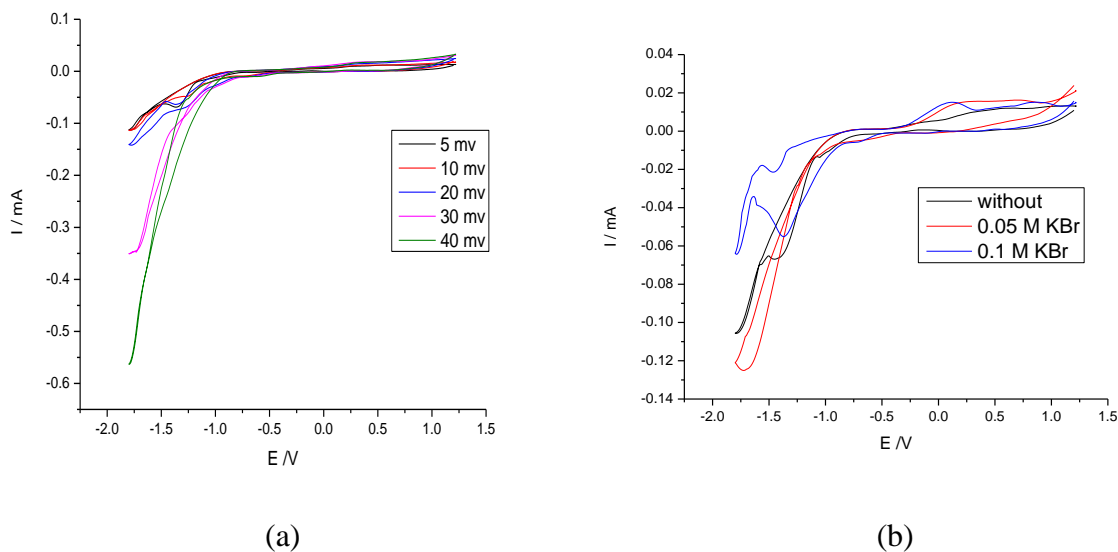


Figure 3. 14: Cyclic voltammograms of $0.7 \text{ mol L}^{-1} \text{ MnCl}_2 \cdot 4\text{H}_2\text{O}$ in Ethaline 200 at 80°C using a Pt disc electrode, Pt flag electrode, and Ag electrode, (a) as function of scan rates, (b) with and without KBr at 5 mV scan rate

3.3.4 Surface analysis

The effect of KBr as an additive on the morphology of Mn films deposited from Ethaline 200 was investigated. **Fig. 3.15** shows the optical images, SEM, and EDX from left to right, respectively, of the Mn films formed from Ethaline 200 in the presence and absence of different concentration of KBr (0.05 and 0.1 mol L^{-1}). The plating was performed on a Cu substrate at 90°C and at potentiostatic conditions (-1.75 V) for 6 h. The Mn deposited from additive-free electrolyte had a dark black powdery film **Fig. 3.15 (a)**. the samples of Mn films prepared with KBr added into the solution show that the surface became more metallic appearance, as per **Fig 3.15 (b)** and **(c)**. The EDX mapping spectrum results shown in **Fig. 3.15** indicates that Mn deposits were affected by the addition of KBr.

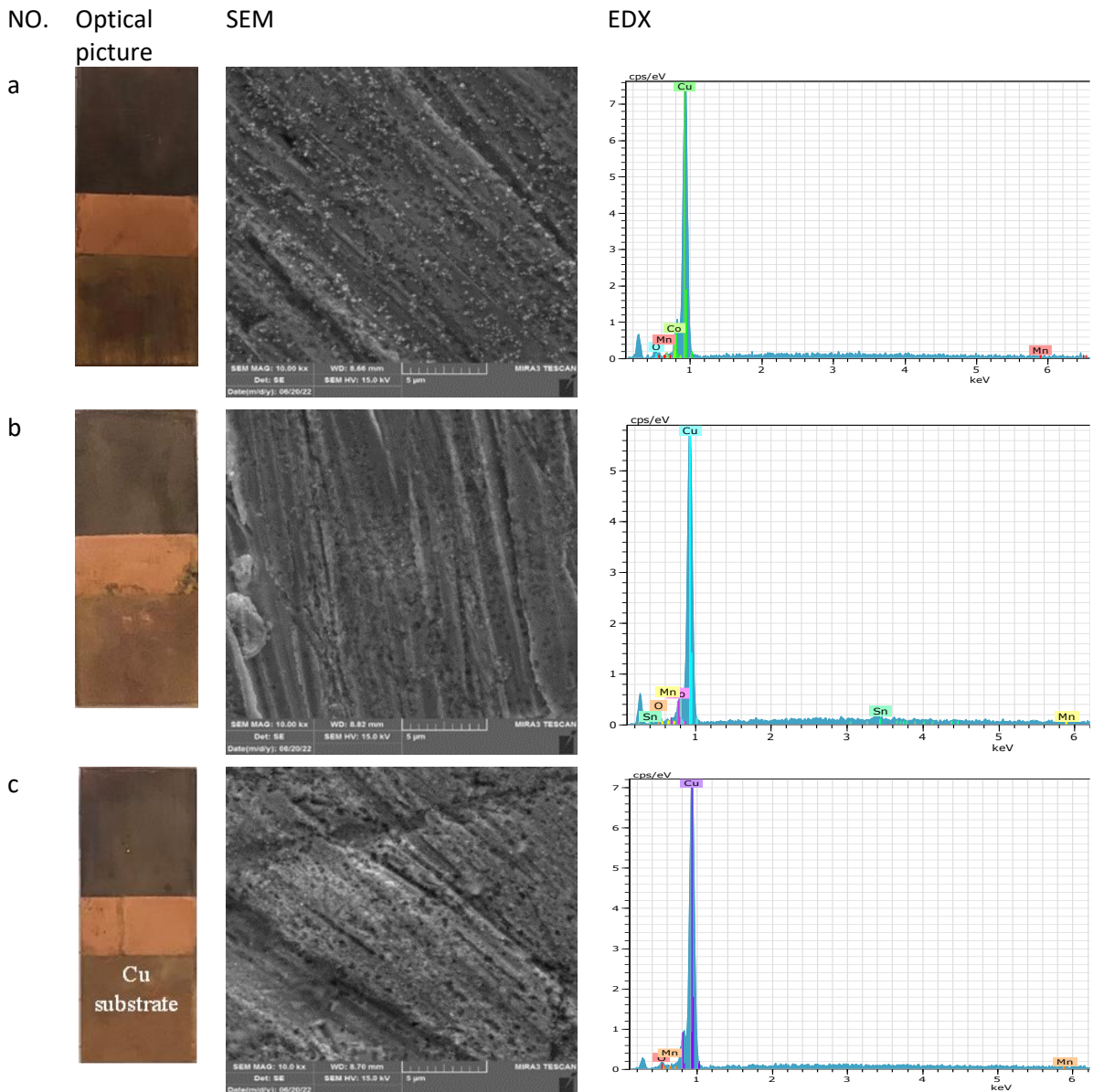


Figure 3. 15: SEM images and EDX spectra showing films electrodeposited from $0.7 \text{ mol L}^{-1} \text{ MnCl}_2 \cdot 4\text{H}_2\text{O}$ in Ethaline 200 systems in the absence and presence of different concentrations of KBr (a) without, (b) with 0.05 mol L^{-1} KBr, and (c) with 0.1 mol L^{-1} KBr

The topographies of the Mn films obtained on the copper substrate with and without additive were found via AFM, as shown in **Fig. 3.16**.

The surface roughness of the electrodeposited Mn films was also characterized via AFM **Table 3.3**, which shows that the average roughness was reduced with increasing KBr concentration.

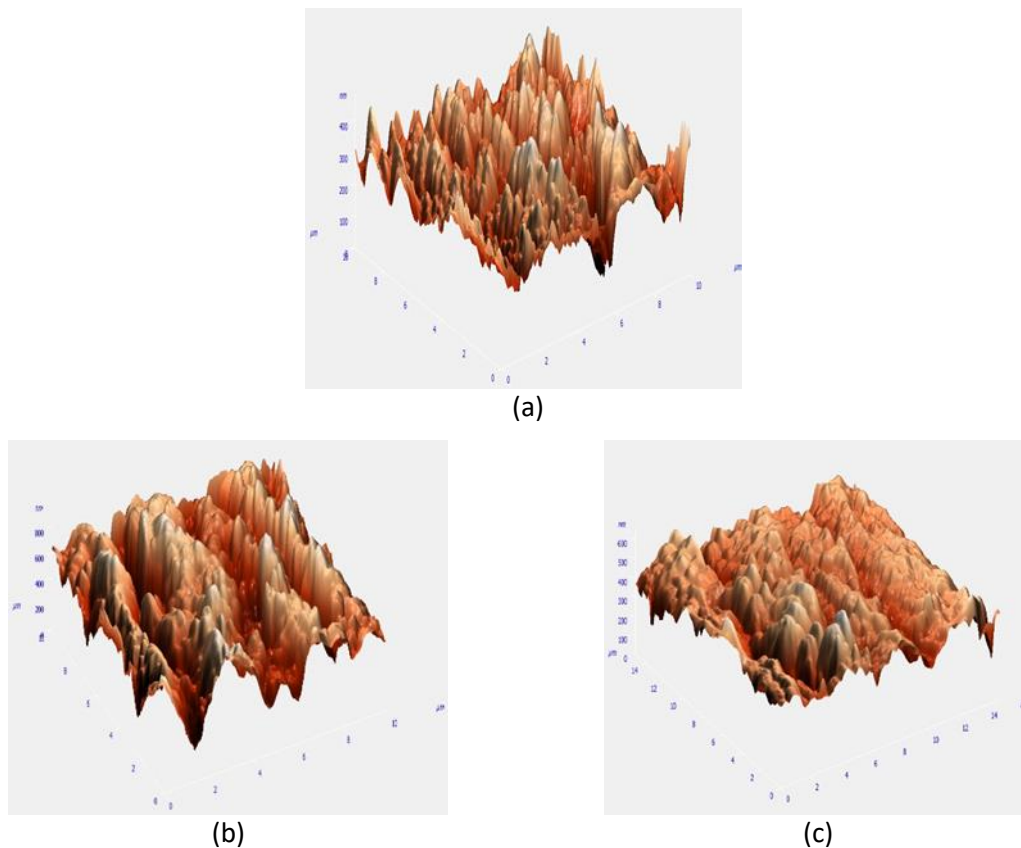


Figure 3. 16: AFM images for the Mn deposit formed from Ethaline 200 (a) without KBr, (b) with 0.05 M KBr, and (c) with 0.1 M KBr

Table 3. 3: Average roughness of the Mn deposits performed from Ethaline 200 containing of different amounts of KBr

Salt	Concentration of KBr, mol L ⁻¹	Average roughness, nm
MnCl ₂ .4H ₂ O	without	46
MnCl ₂ .4H ₂ O	0.05	40
MnCl ₂ .4H ₂ O	0.1	33

XRD analysis was carried out to study the crystal structures of the Mn films obtained on the copper substrate in the absence and presence of KBr at 90°C and a constant potential at 1.75 V, as shown in **Fig. 3.17**. All of the diffraction peaks appearing in **Fig 3.17** at Bragg angles of 43.35°, 50.49°, and 74.19° are associated with the Cu substrate with no other diffraction peaks observed. This indicates that the amorphous nature of the Mn films or because formed very thin film of Mn. This result correlated well with those reported by Guo et al. [56]. Also, no clear change in the XRD patterns was observed with the addition of KBr.

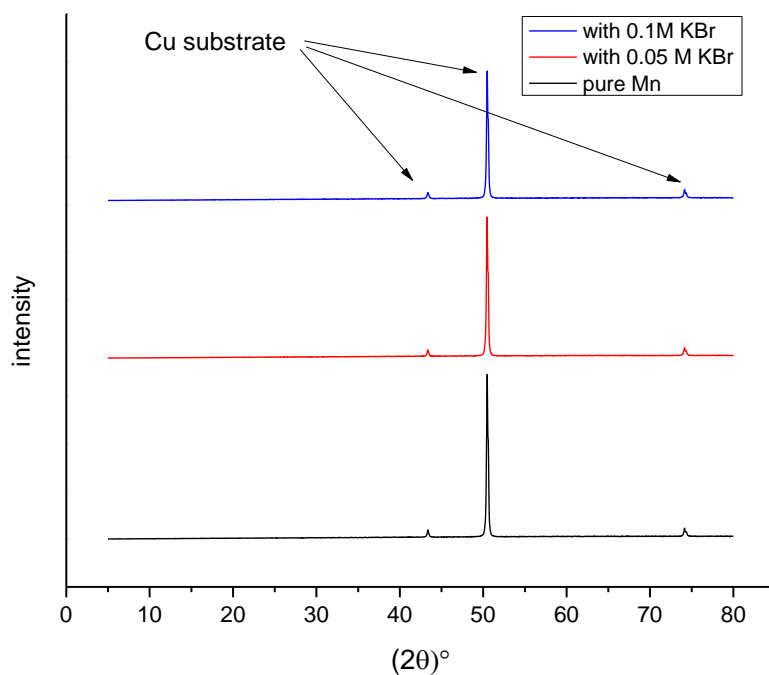


Figure 3. 17: XRD patterns for Mn deposits produced from 0.7 mol L⁻¹ MnCl₂·4H₂O in Ethaline 200 with 0.05 mol L⁻¹ and 0.1 mol L⁻¹ KBr. All deposits were performed for 6 h. at 90 °C and at a constant potential of -1.75 V.

3.4 Conclusions

In this study the electrodeposition of Ag, Sn, and Mn have been achieved from 1:2 ChCl:EG as deep eutectic solvent. The effect of some factors such as temperature, additives and substrate on the electrodeposition process of these metals have also been considered.

The electrochemical behavior of above mentioned elements in the deep eutectic solvent Ethaline 200 have been studied by using cyclic voltammetry technique. Cyclic voltammetry measurements of Sn appear a slight decrease in the Sn deposition peak when BA was added to the Sn electrolyte. Which is due to the adsorption of BA on to the surface electrode, inhibiting Sn deposition.

It was found that there was a notable change in the intensity of oxidation and reduction peaks of Ag at the high temperature (80 °C) compared with those measured at lower temperature due to increase the free volumes in solution, decrease the viscosity and decrease the Cl⁻ anions that adsorbed on the electrode, which lead to increase the velocity of oxidation- reduction processes.

In the cyclic voltammetry measurements of manganese, it was found that no clear oxidation peak for Mn may have been due to the instability of the Mn deposits, which readily oxidized in the electrolyte.

The surface morphology, topography and crystal structure of the Ag, Sn, and Mn films were carried out using SEM, AFM, and XRD techniques respectively. The SEM results showed considerable improvement of Sn films when adding boric acid to the plating bath. This is a result of the decreased crystal size due to the adding of various concentrations of BA as inorganic additive. This presumes that BA may work because the grain is smaller for film deposition, which would lead to a lowering in growth rate of the Sn deposit.

The morphology of Mn films seems to be effected by addition of KBr to plating bath. The XRD data showed that the nature of the Mn films obtained on copper substrate is an amorphous. However further work must be done to investigate the electrodeposition of pure Mn from DESs.

3.5 Future work

1- The effects of the additives used in this project, namely boric acid, potassium bromide, on the electrodeposition of different types of metal such as Co, Cr, Pb, and Bi from Ethaline 200 as a DES. Moreover, the effects of other types of additives, such as polyethyleneglycol, sorbitol, coumarin, vanillin and nicotinamide on the electrodeposition of Sn, Ag and Mn from Ethaline 200 can also be studied.

2- The effects of the additives mentioned in point (1) on the electrodeposition of Zn-Ni, Zn-Sn, Zn-Co, Zn-Cu, and Sn-Mn alloys from Ethaline 200.

3- The effects of the additives mentioned in point (1) on the electrodeposition of metals and metal alloys from reline (1:2 molar mixture of choline chloride and urea) as a deep eutectic solvent

References

1. Giurlani, W., G. Zangari, F. Gambinossi, M. Passaponti, E. Salvietti, F. Di Benedetto, S. Caporali, and M. Innocenti, *Electroplating for decorative applications: Recent trends in research and development*. Coatings, 2018. **8**(8): p. 260.
2. Zangari, G., *Electrodeposition of alloys and compounds in the era of microelectronics and energy conversion technology*. Coatings, 2015. **5**(2): p. 195-218.
3. Bernasconi, R., G. Panzeri, A. Accogli, F. Liberale, L. Nobili, and L. Magagnin, *Electrodeposition from deep eutectic solvents*. Intech. Prog. Dev. Lon. Liq, 2017: p. 235-261.
4. Alesary, H.F., A.F. Khudhair, S.Y. Rfaish, and H.K. Ismail, *Effect of sodium bromide on the electrodeposition of Sn, Cu, Ag and Ni from a deep eutectic solvent-based ionic liquid*. Int J Electrochem Sci, 2019. **14**: p. 7116-7132.
5. Abbott, A.P., G. Frisch, and K.S. Ryder, *Electroplating using ionic liquids*. Annual Review of Materials Research, 2013. **43**: p. 335-358.
6. Bodo, E. and V. Migliorati, *Theoretical Description of Ionic Liquids*. Ionic Liquids-Classes and Properties, 2011. **1**.
7. Kudłak, B., K. Owczarek, and J. Namieśnik, *Selected issues related to the toxicity of ionic liquids and deep eutectic solvents—a review*. Environmental Science and Pollution Research, 2015. **22**(16): p. 11975-11992.
8. Pena-Pereira, F. and J. Namieśnik, *Ionic liquids and deep eutectic mixtures: sustainable solvents for extraction processes*. ChemSusChem, 2014. **7**(7): p. 1784-1800.
9. Shamsuri, A.A., *Ionic liquids: preparations and limitations*. Makara Journal of Science, 2011.
10. Abbott, A.P. and K.J. McKenzie, *Application of ionic liquids to the electrodeposition of metals*. Physical Chemistry Chemical Physics, 2006. **8**(37): p. 4265-4279.
11. Marcus, Y., *The Variety of Deep Eutectic Solvents*, in *Deep Eutectic Solvents*. 2019, Springer International Publishing: Cham. p. 13-44.

12. Abbott, A.P., G. Capper, D.L. Davies, R.K. Rasheed, and V. Tambyrajah, *Novel solvent properties of choline chloride/urea mixtures*. Chemical communications, 2003(1): p. 70-71.
13. Tang, B., H. Zhang, and K.H. Row, *Application of deep eutectic solvents in the extraction and separation of target compounds from various samples*. Journal of separation science, 2015. **38**(6): p. 1053-1064.
14. Alizadeh, V., F. Malberg, A.A. Pádua, and B. Kirchner, *Are there magic compositions in deep eutectic solvents? Effects of composition and water content in choline chloride/ethylene glycol from ab initio molecular dynamics*. The Journal of Physical Chemistry B, 2020. **124**(34): p. 7433-7443.
15. Kollau, L.J., M. Vis, A. Van Den Bruinhorst, and R. Tuinier, *Activity modelling of the solid–liquid equilibrium of deep eutectic solvents*. Pure and Applied Chemistry, 2019. **91**(8): p. 1341-1349.
16. Hansen, B.B., S. Spittle, B. Chen, D. Poe, Y. Zhang, J.M. Klein, A. Horton, L. Adhikari, T. Zelovich, and B.W. Doherty, *Deep eutectic solvents: A review of fundamentals and applications*. Chemical reviews, 2020. **121**(3): p. 1232-1285.
17. Płotka-Wasyłka, J., M. De la Guardia, V. Andruch, and M. Vilková, *Deep eutectic solvents vs ionic liquids: Similarities and differences*. Microchemical Journal, 2020. **159**: p. 105539.
18. Wen, Q., J.-X. Chen, Y.-L. Tang, J. Wang, and Z. Yang, *Assessing the toxicity and biodegradability of deep eutectic solvents*. Chemosphere, 2015. **132**: p. 63-69.
19. Zhekenov, T., N. Toksanbayev, Z. Kazakbayeva, D. Shah, and F.S. Mjalli, *Formation of type III Deep Eutectic Solvents and effect of water on their intermolecular interactions*. Fluid Phase Equilibria, 2017. **441**: p. 43-48.
20. Tomé, L.I., V. Baião, W. da Silva, and C.M. Brett, *Deep eutectic solvents for the production and application of new materials*. Applied Materials Today, 2018. **10**: p. 30-50.
21. Al-Murshedi, A.Y.M., *Deep eutectic solvent-water mixtures*, PhD Thesis. 2018, University of Leicester.

22. Smith, E.L., A.P. Abbott, and K.S. Ryder, *Deep eutectic solvents (DESs) and their applications*. Chemical reviews, 2014. **114**(21): p. 11060-11082.
23. El Achkar, T., H. Greige-Gerges, and S. Fourmentin, *Basics and properties of deep eutectic solvents: a review*. Environmental Chemistry Letters, 2021. **19**(4): p. 3397-3408.
24. Leron, R.B. and M.-H. Li, *High-pressure volumetric properties of choline chloride–ethylene glycol based deep eutectic solvent and its mixtures with water*. Thermochimica acta, 2012. **546**: p. 54-60.
25. Zhang, Y., D. Poe, L. Heroux, H. Squire, B.W. Doherty, Z. Long, M. Dadmun, B. Gurkan, M.E. Tuckerman, and E.J. Maginn, *Liquid structure and transport properties of the deep eutectic solvent ethaline*. The Journal of Physical Chemistry B, 2020. **124**(25): p. 5251-5264.
26. Lapeña, D., L. Lomba, M. Artal, C. Lafuente, and B. Giner, *Thermophysical characterization of the deep eutectic solvent choline chloride: ethylene glycol and one of its mixtures with water*. Fluid Phase Equilibria, 2019. **492**: p. 1-9.
27. Kaur, S., A. Malik, and H.K. Kashyap, *Anatomy of microscopic structure of ethaline deep eutectic solvent decoded through molecular dynamics simulations*. The Journal of Physical Chemistry B, 2019. **123**(39): p. 8291-8299.
28. Alesary, H.F., H.K. Ismail, N.M. Shiltagh, R.A. Alattar, L.M. Ahmed, M.J. Watkins, and K.S. Ryder, *Effects of additives on the electrodeposition of ZnSn alloys from choline chloride/ethylene glycol-based deep eutectic solvent*. Journal of Electroanalytical Chemistry, 2020. **874**: p. 114517.
29. Marcus, Y., *Applications of deep eutectic solvents*, in *Deep Eutectic Solvents*. 2019, Springer. p. 111-151.
30. Huang, X., Y. Chen, T. Fu, Z. Zhang, and J. Zhang, *Study of tin electroplating process using electrochemical impedance and noise techniques*. Journal of the Electrochemical Society, 2013. **160**(11): p. D530.
31. Sekar, R., C. Eagammai, and S. Jayakrishnan, *Effect of additives on electrodeposition of tin and its structural and corrosion behaviour*. Journal of Applied Electrochemistry, 2010. **40**(1): p. 49-57.

32. Han, C., Q. Liu, and D.G. Ivey, *Nucleation of Sn and Sn–Cu alloys on Pt during electrodeposition from Sn–citrate and Sn–Cu–citrate solutions*. *Electrochimica Acta*, 2009. **54**(12): p. 3419-3427.
33. Pewnim, N. and S. Roy, *Effect of fluorosurfactant on copper–tin reduction from methanesulphonic acid electrolyte*. *Transactions of the IMF*, 2011. **89**(4): p. 206-209.
34. Vieira, L., J. Burt, P.W. Richardson, D. Schloffer, D. Fuchs, A. Moser, P.N. Bartlett, G. Reid, and B. Gollas, *Tin, bismuth, and tin–bismuth alloy electrodeposition from chlorometalate salts in deep eutectic solvents*. *ChemistryOpen*, 2017. **6**(3): p. 393-401.
35. Tachikawa, N., N. Serizawa, Y. Katayama, and T. Miura, *Electrochemistry of Sn (II)/Sn in a hydrophobic room-temperature ionic liquid*. *Electrochimica Acta*, 2008. **53**(22): p. 6530-6534.
36. Leong, T.-I., Y.-T. Hsieh, and I.-W. Sun, *Electrochemistry of tin in the 1-ethyl-3-methylimidazolium dicyanamide room temperature ionic liquid*. *Electrochimica Acta*, 2011. **56**(11): p. 3941-3946.
37. Zhang, Q., K.D.O. Vigier, S. Royer, and F. Jérôme, *Deep eutectic solvents: syntheses, properties and applications*. *Chemical Society Reviews*, 2012. **41**(21): p. 7108-7146.
38. Shishov, A., A. Bulatov, M. Locatelli, S. Carradori, and V. Andrich, *Application of deep eutectic solvents in analytical chemistry. A review*. *Microchemical Journal*, 2017. **135**: p. 33-38.
39. Alesary, H.F., H.K. Ismail, M.Q. Mohammed, H.N. Mohammed, Z.K. Abbas, and S. Barton, *A comparative study of the effect of organic dopant ions on the electrochemical and chemical synthesis of the conducting polymers polyaniline, poly (o-toluidine) and poly (o-methoxyaniline)*. *Chemical Papers*, 2021. **75**(10): p. 5087-5101.
40. Alesary, H.F., S. Cihangir, A.D. Ballantyne, R.C. Harris, D.P. Weston, A.P. Abbott, and K.S. Ryder, *Influence of additives on the electrodeposition of zinc from a deep eutectic solvent*. *Electrochimica Acta*, 2019. **304**: p. 118-130.
41. Al-Murshedi, A.Y., A. Al-Yasari, H.F. Alesary, and H.K. Ismail, *Electrochemical fabrication of cobalt films in a choline chloride–ethylene glycol deep eutectic solvent containing water*. *Chemical Papers*, 2020. **74**(2): p. 699-709.

42. Ismail, H.K., H.F. Alesary, A.Y. Al-Murshedi, and J.H. Kareem, *Ion and solvent transfer of polyaniline films electrodeposited from deep eutectic solvents via EQCM*. Journal of Solid State Electrochemistry, 2019. **23**(11): p. 3107-3121.
43. Lei, C., H.F. Alesary, F. Khan, A.P. Abbott, and K.S. Ryder, *Gamma-phase Zn-Ni alloy deposition by pulse-electroplating from a modified deep eutectic solution*. Surface and Coatings Technology, 2020. **403**: p. 126434.
44. Alesary, H.F., H.K. Ismail, A.H. Odda, M.J. Watkins, A.A. Majhool, A.D. Ballantyne, and K.S. Ryder, *Influence of different concentrations of nicotinic acid on the electrochemical fabrication of copper film from an ionic liquid based on the complexation of choline chloride-ethylene glycol*. Journal of Electroanalytical Chemistry, 2021. **897**: p. 115581.
45. Mohammed, M.Q., A.M. Jassem, J.M. Al-Shawi, and H.F. Alesary. *Comparative electrochemical behavior of poly (3-aminobenzoic acid) films in conventional and non-conventional solvents*. in *AIP Conference Proceedings*. 2020. AIP Publishing LLC.
46. Ismail, H.K., H.F. Alesary, and M.Q. Mohammed, *Synthesis and characterisation of polyaniline and/or MoO₂/graphite composites from deep eutectic solvents via chemical polymerisation*. Journal of Polymer Research, 2019. **26**(3): p. 1-12.
47. Al-Murshedi, A.Y.M., H.F. Alesary, and R. Al-Hadrawi. *Thermophysical properties in deep eutectic solvents with/without water*. in *Journal of Physics: Conference Series*. 2019. IOP Publishing.
48. Alesary, H.F., H.K. Ismail, A.F. Khudhair, and M.Q. Mohammed, *Effects of dopant ions on the properties of polyaniline conducting polymer*. Oriental Journal of Chemistry, 2018. **34**(5): p. 2525.
49. Gu, C., Y. Mai, J. Zhou, Y. You, and J. Tu, *Non-aqueous electrodeposition of porous tin-based film as an anode for lithium-ion battery*. Journal of Power Sources, 2012. **214**: p. 200-207.
50. Salomé, S., N.M. Pereira, E.S. Ferreira, C.M. Pereira, and A. Silva, *Tin electrodeposition from choline chloride based solvent: Influence of the hydrogen bond donors*. Journal of Electroanalytical Chemistry, 2013. **703**: p. 80-87.
51. Ghosh, S. and S. Roy, *Characterization of tin films synthesized from ethaline deep eutectic solvent*. Materials Science and Engineering: B, 2014. **190**: p. 104-110.

52. Cao, X., L. Xu, C. Wang, S. Li, D. Wu, Y. Shi, F. Liu, and X. Xue, *Electrochemical behavior and electrodeposition of Sn coating from choline chloride–urea deep eutectic solvents*. *Coatings*, 2020. **10**(12): p. 1154.
53. Bomparola, R., S. Caporali, A. Lavacchi, and U. Bardi, *Silver electrodeposition from air and water-stable ionic liquid: An environmentally friendly alternative to cyanide baths*. *Surface and Coatings Technology*, 2007. **201**(24): p. 9485-9490.
54. Basile, A., A.I. Bhatt, A.P. O'Mullane, and S.K. Bhargava, *An investigation of silver electrodeposition from ionic liquids: Influence of atmospheric water uptake on the silver electrodeposition mechanism and film morphology*. *Electrochimica acta*, 2011. **56**(7): p. 2895-2905.
55. Rahali, S., R. Zarrougui, M. Marzouki, and O. Ghodbane, *Electrodeposition of silver from the ionic liquid Butylpyridinium dicyanamide*. *Journal of Electroanalytical Chemistry*, 2020. **871**: p. 114289.
56. Guo, M., C. Sun, W. Yang, L. Chen, H. Lei, and Q. Zhang, *Sulphur-induced electrochemical synthesis of manganese nanoflakes from choline chloride/ethylene glycol-based deep eutectic solvent*. *Electrochimica Acta*, 2020. **341**: p. 136017.
57. Chen, J., B. Xu, and G. Ling, *Amorphous Al–Mn coating on NdFeB magnets: Electrodeposition from AlCl₃–EMIC–MnCl₂ ionic liquid and its corrosion behavior*. *Materials Chemistry and Physics*, 2012. **134**(2-3): p. 1067-1071.
58. Guo, J., X. Guo, S. Wang, Z. Zhang, J. Dong, L. Peng, and W. Ding, *Effects of glycine and current density on the mechanism of electrodeposition, composition and properties of Ni–Mn films prepared in ionic liquid*. *Applied Surface Science*, 2016. **365**: p. 31-37.
59. Fashu, S., C. Gu, J. Zhang, H. Zheng, X. Wang, and J. Tu, *Electrodeposition, morphology, composition, and corrosion performance of Zn–Mn coatings from a deep eutectic solvent*. *Journal of Materials Engineering and Performance*, 2015. **24**(1): p. 434-444.
60. Lu, J., D. Dreisinger, and T. Glück, *Manganese electrodeposition—a literature review*. *Hydrometallurgy*, 2014. **141**: p. 105-116.
61. Zhang, X., X. Zhang, Z. Liu, C. Tao, and X. Quan, *Pulse current electrodeposition of manganese metal from sulfate solution*. *Journal of Environmental Chemical Engineering*, 2019. **7**(2): p. 103010.

62. Zhuang, D.-X., M.-J. Deng, P.-Y. Chen, and I.-W. Sun, *Electrochemistry of manganese in the hydrophilic N-butyl-N-methylpyrrolidinium dicyanamide room-temperature ionic liquid*. Journal of The Electrochemical Society, 2008. **155**(9): p. D575.
63. Chang, J.-K., C.-H. Huang, W.-T. Tsai, M.-J. Deng, I.-W. Sun, and P.-Y. Chen, *Manganese films electrodeposited at different potentials and temperatures in ionic liquid and their application as electrode materials for supercapacitors*. Electrochimica Acta, 2008. **53**(13): p. 4447-4453.
64. Deng, M.-J., P.-Y. Chen, and I.-W. Sun, *Electrochemical study and electrodeposition of manganese in the hydrophobic butylmethylpyrrolidinium bis ((trifluoromethyl) sulfonyl) imide room-temperature ionic liquid*. Electrochimica Acta, 2007. **53**(4): p. 1931-1938.
65. Bozzini, B., A. Gianoncelli, B. Kaulich, C. Mele, M. Prasciolu, and M. Kiskinova, *Electrodeposition of manganese oxide from eutectic urea/choline chloride ionic liquid: An in situ study based on soft X-ray spectromicroscopy and visible reflectivity*. Journal of Power Sources, 2012. **211**: p. 71-76.
66. Padhy, S.K., B.C. Tripathy, and A. Alfantazi, *Effect of sodium alkyl sulfates on electrodeposition of manganese metal from sulfate solutions in the presence of sodium metabisulphite*. Hydrometallurgy, 2018. **177**: p. 227-236.
67. Sides, W.D. and Q. Huang, *Electrodeposition of manganese thin films on a rotating disk electrode from choline chloride/urea based ionic liquids*. Electrochimica Acta, 2018. **266**: p. 185-192.
68. Azam, M., *The electrochemistry of Ag in deep eutectic solvents*, PhD Thesis. 2012, University of Leicester.
69. Gamburg, Y.D. and G. Zangari, *Theory and practice of metal electrodeposition*. 2011: Springer Science & Business Media.
70. Alcanfor, A.A., L.P. dos Santos, D.F. Dias, A.N. Correia, and P. de Lima-Neto, *Electrodeposition of indium on copper from deep eutectic solvents based on choline chloride and ethylene glycol*. Electrochimica Acta, 2017. **235**: p. 553-560.
71. Al-Esary, H.F.N., *Influence of additives on electrodeposition of metals from deep eutectic solvents*, PhD Thesis. 2017, University of Leicester.

72. Schlesinger, M. and M. Paunovic, *Modern electroplating*. 2011: John Wiley & Sons.
73. Oniciu, L. and L. Mureşan, *Some fundamental aspects of levelling and brightening in metal electrodeposition*. Journal of applied electrochemistry, 1991. **21**(7): p. 565-574.
74. Langhus, D.L., *Analytical Electrochemistry*, (Wang, Joseph). 2001, ACS Publications.
75. Abd Mutalib, M., M. Rahman, M. Othman, A. Ismail, and J. Jaafar, *Scanning electron microscopy (SEM) and energy-dispersive X-ray (EDX) spectroscopy*, in *Membrane characterization*. 2017, Elsevier. p. 161-179.
76. Mishra, R.K., A.K. Zachariah, and S. Thomas, *Energy-dispersive X-ray spectroscopy techniques for nanomaterial*, in *Microscopy Methods in Nanomaterials Characterization*. 2017, Elsevier. p. 383-405.
77. Eaton, P. and P. West, *Atomic force microscopy*. 2010: Oxford university press.
78. Bunaciu, A.A., E.G. UdrişTioiu, and H.Y. Aboul-Enein, *X-ray diffraction: instrumentation and applications*. Critical reviews in analytical chemistry, 2015. **45**(4): p. 289-299.
79. Wang, H., Y. Jia, X. Wang, Y. Yao, and Y. Jing, *Physical–chemical properties of nickel analogs ionic liquid based on choline chloride*. Journal of Thermal Analysis and Calorimetry, 2013. **115**(2): p. 1779-1785.
80. Lu, Y.-S., W.-Y. Pan, T.-C. Hung, and Y.-T. Hsieh, *Electrodeposition of silver in a ternary deep eutectic solvent and the electrochemical sensing ability of the Ag-modified electrode for nitrofurazone*. Langmuir, 2020. **36**(38): p. 11358-11365.
81. Hartley, J.M., C.-M. Ip, G.C. Forrest, K. Singh, S.J. Gurman, K.S. Ryder, A.P. Abbott, and G. Frisch, *EXAFS study into the speciation of metal salts dissolved in ionic liquids and deep eutectic solvents*. Inorganic chemistry, 2014. **53**(12): p. 6280-6288.
82. Pereira, N.M., C.M. Pereira, J.P. Araújo, and A.F. Silva, *Electrodeposition of Mn and Mn-Sn Alloy Using Choline Chloride-Based Ionic Liquids*. Journal of the Electrochemical Society, 2017. **164**(7): p. D486.
83. Tariq, M., *Electrochemistry of Br⁻/Br₂ Redox Couple in Acetonitrile, Methanol and Mix Media of Acetonitrile–Methanol: An Insight into Redox Behavior of Bromide on Platinum (Pt) and Gold (Au) Electrode*. Zeitschrift für Physikalische Chemie, 2020. **234**(2): p. 295-312.

الخلاصة

ان عملية الترسيب الكهربائي للمعادن لها اهمية في صناعات السيارات والطيران. يمكن تحسين الخواص الفيزيائية والميكانيكية للأدوات المعدنية عن طريق الترسيب بالمعادن التي تتمتع بمقاومة عالية للتآكل. يتم استخدام Sn و Ag و Mn بشكل عام للحماية من التآكل للألواح الفولاذية أو القطع المعدنية الأخرى. تم تحقيق الترسيب الكهربائي للمعادن سابقاً في محلول مائي. ومع ذلك ، فإن عيوب المحاليل المائية حدثت من ترسب المعادن. كان الهدف الرئيسي من هذه الدراسة هو استخدام المذيب الأخضر (Ethaline200) أثناء الترسيب الكهربائي لـ Sn و Ag و Mn مع تحسين جودة الطلاء باستخدام المواد المضافة. في هذا العمل تم دراسة تأثير درجة الحرارة والمواد المضافة على الترسيب الكهربائي لكل من Sn و Ag و Mn من Ethaline 200. وجد أن ارتفاع درجة الحرارة يؤثر بشكل كبير على شكل رواسب Sn حيث ينتج غشاء متجانس. حسّن حمض البوريك (BA) من مورفولوجيا Sn. علاوة على ذلك ، تم تحقيق الترسيب الكهربائي لـ Sn على ركيزة معدنية مختلفة (النحاس والفولاذ الطري والنحاس الأصفر). تمت دراسة الترسيب الكهربائي لـ Ag من Ethaline 200 (1ChCl: 2EG) على ركيزة معدنية مختلفة (النحاس والفولاذ الطري). وجد أن نوع الركيزة أثر بشكل كبير على رواسب Ag.

تم فحص تأثيرات بروميد البوتاسيوم (KBr) كمادة مضافة غير عضوية على الترسيب الكهربائي للمنغنيز من إيثالين 200 ، ويمكن إظهار التحسين في ترسب المنغنيز. تمت دراسة الخواص الكهروكيميائية لسائل الطلاء باستخدام مقياس الجهد الدوري وتم الكشف عن خصائص السطح الناتجة مثل الشكل والتركيب والسمك بواسطة SEM / EDXS و AFM. تم استخدام XRD لفحص التركيب البلوري لـ Sn و Ag و Mn.



جامعة كربلاء
كلية العلوم
قسم الكيمياء

الطلاء الكهربائي ل Ag و Sn و Mn من السوائل الايونية

رسالة مقدمة الى

مجلس كلية العلوم – جامعة كربلاء

كجزء من استكمال متطلبات نيل درجة الماجستير

علوم في الكيمياء

تقدمت بها

ضحى يحيى نوري

بكالوريوس علوم في الكيمياء (2019) جامعة كربلاء

باشرف

ا.م.د حسن فيصل نعمة
ا.م.د احمد هادي عبد الامير